Journal of Manufacturing Systems 77 (2024) 246–265

Contents lists available at ScienceDirect

Journal of Manufacturing Systems

journal homepage: www.elsevier.com/locate/jmansys

Technical paper

Digital ergonomic assessment to enhance the physical resilience of human-centric manufacturing systems in Industry 5.0

Federica Tomelleri [a,*], Andrea Sbaragli [a], Francesco Picariello [b], Francesco Pilati [a]

[a] Department of Industrial Engineering, University of Trento, Via Sommarive 9, Trento, 38123, Italy
[b] Department of Engineering, University of Sannio, Piazza Guerrazzi, Benevento, 82100, Italy

ARTICLE INFO

Keywords:
Industry 5.0
Human-centric
IoT
EAWS
Physical resilience

ABSTRACT

The emergence of Industry 5.0 promotes the creation of human-centric values. To fulfill this objective, Internet of Things (IoT) technologies are increasingly being exploited to digitize the human factor and monitor the ergonomics of manual manufacturing systems. These digital assessments, combined with computational algorithms, contribute to the establishment of socially inclusive workplaces while offering detailed insights to safeguard the health of the aging workforce. In this scenario, this study proposes a digital architecture for evaluating the European Assembly Worksheet (EAWS) in human-centric manufacturing systems. Three distinct enabling technologies are leveraged to acquire heterogeneous data streams. A radio-frequency-based smart glove detects the operator's interactions with the surrounding environment, while a network of markerless cameras and a four-channel surface Electromyography (sEMG) system capture body joint movements and muscular contractions of the upper limbs, respectively. The acquired data are processed by computational algorithms to define an EAWS-driven set of Key Risk Indicators (KRIs), embedded in an ergonomic decision support system. These risk metrics highlight operator-driven process weaknesses in musculoskeletal, muscular, and material handling dimensions. Finally, the validity of the proposed digital architecture is demonstrated in an industrial-related pilot environment, where an operator assembles a piece of home furniture.

1. Introduction

In recent years, the manufacturing landscape has faced various disruptions, ranging from social to market threats [1]. On the one hand, the European population is experiencing a concerning trend in aging, leading to a significant reduction in the workforce. According to Eurostat projections, individuals aged 55 years or older will peak at 40.6% of the European population by 2050, up from 33.6% in 2019 [2]. Simultaneously, high turnover rates in jobs contribute to increased manufacturing costs related to operator training and replacement [3]; this rate for trade workers reached 7.8% in 2021 [4]. On the other hand, customer preferences are steering smart factories toward offering high production flexibility with shorter product life cycles [5,6]. Consequently, traditional managerial approaches prove insufficient for efficiently monitoring complex processes in mass-customized markets [7].

To mitigate these threats and ensure long-term market competitiveness, industrial environments have widely adopted process automation, Internet of Things (IoT) technologies, and data analytics. For instance, robotic arms are extensively used to ensure the safety and well-being of workers in various manufacturing tasks, ranging from picking operations to handling hazardous activities [8]. Additionally, [9] demonstrates how to automate the quality inspection of finished goods, enhancing system responsiveness and efficiency. Other valuable approaches utilize IoT sensors to monitor process traceability [10,11]. However, the value creation of Industry 4.0 focuses on enhancing productivity and performance, failing to address significant European societal and demographic changes [1,12]. Still, the human factor remains crucial in adding value to in-plant operations and represents one of the most flexible resources, particularly in small and medium enterprises [3,13]. Consequently, the Industry 5.0 paradigm is gaining traction by integrating social and environmental drivers into technological innovation [1,14]. This shift emphasizes a systematic approach that places human-centricity, sustainability, and resilience as core features of modern manufacturing systems [15]. This novel paradigm introduces a techno-social revolution, where technology serves as an enabling tool, while societal needs drive industrial value creation [12,16].

Based on this, investigating the human factor is essential to achieving operator-centric and socially sustainable manufacturing processes [17–19]. The Operator 5.0 concept promotes IoT-based investigations to assist and augment workers' capabilities and skills while safeguarding their self-resilience during value-added activities [20]. Among

* Corresponding author.
E-mail address: federica.tomelleri@unitn.it (F. Tomelleri).

https://doi.org/10.1016/j.jmsy.2024.09.003
Received 26 February 2024; Received in revised form 10 September 2024; Accepted 11 September 2024
Available online 26 September 2024

the different dimensions of self-resilience, physical and occupational health represent pivotal areas of application [21]. Physical resilience is defined as workers' ability to maintain stamina and strength over time [18]. Various research contributions have been tested and validated in this field, where IoT-based methodologies are preferred over conventional managerial approaches [13]. Motion Capture (MOCAP) technologies and surface Electromyography (sEMG) wearables are widely used to assess potential musculoskeletal disorders and hazardous muscular efforts during manual manufacturing processes [22,23]. These parameters can be used to automate the development of ergonomic indices such as the European Assembly Worksheet (EAWS) [24]. Despite this, the literature falls short in digitizing multiple EAWS sections with a set of enabling IoT technologies.

Based on this limitation and the ever-evolving manufacturing landscape, this manuscript proposes an original digital architecture to assess process and operator-centric EAWS assessments. To achieve this goal, three IoT technologies capture physiological and process-driven data streams to evaluate the first three EAWS sections, namely Basic Postures, Action Forces, and Manual Material Handling. A Radio Frequency Identification (RFID)-based smart glove records Operator-Process Interactions (OPIs), while a network of MOCAP cameras and surface Electromyography (sEMG) wearables captures human body joints and muscular contractions of workers during task execution. Computational algorithms leverage this heterogeneous information to automatically evaluate a set of EAWS-informed Key Risk Indicators (KRIs) to analyze the safety weaknesses of human-centric manufacturing processes. The outputs are embedded in an ergonomic Decision Support System (DSS) to provide industrial plant supervisors with a user-friendly and effective tool to safeguard operators' physical resilience.

This paper is structured as follows. Section 2 explores human-centric production environments during the Industry 5.0 era, along with IoT-based approaches to safeguard operators' well-being. The novelty of this work is presented in Section 3, where the IoT-based architecture to digitize the EAWS index is introduced. This solution is validated in an industrial-related pilot environment, described in Section 4. Section 5 illustrates how the obtained multidimensional KRIs effectively identify safety weaknesses in human-centric manufacturing systems, while Section 6 concludes this work, outlining the findings and suggesting further research opportunities.

2. Literature review

The recent emergence of Industry 5.0 underscores the strategic collaboration between technology and human workers as a primary goal in modern manufacturing systems [18,25]. Among various enabling technologies, IoT sensors facilitate data acquisition and insightful process monitoring [9,13]. Industrial systems can enhance operational resilience by dynamically adjusting their in-plant functioning in response to unexpected working conditions, thus fostering mutual collaboration between workers and automation [26]. For instance, motion, positioning, and environmental sensors are widely employed to prevent production stoppages and mitigate work-related injuries [27,28]. Simultaneously, IoT-driven monitoring of the human factor contributes to the establishment of the Operator 5.0 concept. This innovative human-centric vision combines technological capabilities with human cognitive abilities to foster socially inclusive manufacturing environments [25]. Internet-connected devices are utilized to safeguard operators' well-being, addressing a spectrum of drivers from emotional to physical aspects, thereby promoting the augmentation of their skills [29]. For example, physiological sensors such as Electroencephalography are extensively investigated to analyze workers' mental workload during task execution [30]. Furthermore, integrating modern technologies with ergonomic assessment tools has proven very effective in addressing the physical dimension.

Ergonomic indices are widely adopted to evaluate physical strain and discomfort in human-centric industrial environments, encompassing a broad range of parameters [31]. For instance, the Occupational Repetitive Actions (OCRA) index assesses the risk of strain injuries, particularly focusing on the upper limbs, while the National Institute for Occupational Safety and Health (NIOSH) proposes a static equation to evaluate musculoskeletal risk during lifting activities [32,33]. Among these standardized ergonomic tools, the EAWS represents the most comprehensive assessment [24].

The EAWS evaluates physical workload in manufacturing environments, particularly in assembly tasks common in the automotive industry. It was created in response to the high prevalence of musculoskeletal complaints and disorders, which account for a significant portion of sick leave in industrialized countries due to poor ergonomic design. The EAWS is divided into four sections, each assessing different aspects of physical workload:

- **Section 0 - General**: Provides a comprehensive overview of the identified workstation, including overall evaluation, rating of additional physical workload, space for comments and improvements, and consideration of time aspects for repetitive loads of the upper limbs.
- **Section 1 - Basic Postures**: Evaluates static postures and repetitive movements with low physical effort. This section considers symmetrical and asymmetrical postures, and the time spent in these movements is counted to assign a score.
- **Section 2 - Action Forces**: Assesses whole-body forces and hand-finger exertions that exceed the threshold of $30-40$ N. Scores are calculated based on the intensity and duration of the force.
- **Section 3 - Manual Materials Handling**: Covers tasks involving loads heavier than $3-4$ kg. It evaluates the weight, posture, working conditions, and frequency of handling activities.
- **Section 4 - Upper Limb Load in Repetitive Tasks**: Focuses on the frequency and duration of repetitive upper limb movements, including forces, gripping modes, and postures. This section is aligned with methodologies from other standards like OCRA.

The EAWS assigns load points for unfavorable physical workload conditions and uses a traffic light scheme (i.e., green, yellow, red) to classify the risk levels. This helps identify ergonomic issues and suggests design improvements.

However, despite the robustness of this tool in evaluating workers' physical resilience during task execution, its implementation and accuracy often rely on conventional managerial approaches, which involve manual data collection and subjective analysis [34]. This can introduce limitations such as human error and time-consuming investigations.

The recent push toward Industry 5.0 emphasizes the need for more advanced and digitally-driven solutions to enhance the efficacy of ergonomic assessments in manufacturing environments. Human involvement and mass-customized production systems may impact the consistency of these indices, affecting the effectiveness of process reconfiguration, which may involve modifications to workstations or equipment [35]. Despite several research contributions exploiting IoT-based digital architectures to trigger ergonomic analysis into a diversified workforce, no investigation leverages enabling IoT technologies to digitize multiple EAWS sections [14,36].

Considering the Basic Posture assessment (i.e., first EAWS section), MOCAP technologies are extensively adopted to digitize operators' movements [37]. Inertial Measurement Units (IMUs) and marker-less MOCAP cameras are the most used IoT devices in human-centric manufacturing systems, despite some operational drawbacks [28,38]. While IMU-based embedded suits are intrusive and require time-consuming calibration processes, marker-less MOCAP cameras represent a low-invasive and easy-to-deploy solution that suffers from potential body occlusions [14,39]. Regardless of the hardware selection, algorithms process the acquired 3D body joints and compute the EAWS posture scores to offer valuable insights into potential musculoskeletal disorders of workers, suggesting reconfiguration strategies. [40] demonstrates that these approaches enhance social inclusion and reduce employee turnover.

However, MOCAP data streams fail to evaluate action or exerted forces (i.e., second EAWS section) during manual task executions, leading to limited investigation of workers' physical resilience. While no digital architectures have been proposed to digitize this second EAWS section, the relevance of investigating action forces in manual assembly is demonstrated by multiple conventional managerial approaches (e.g., workers' reports or ergonomist evaluations) [41–43]. For instance, [42] benchmarks Strain Index (SI) and OCRA Checklist in 10 manual tasks. At the same time, contributions in other research domains leverage sEMG wearables to monitor muscular strength and activity [44]. The sEMG-based muscular contractions are fed into computational algorithms to detect strain and fatigue [14,45]. Although these parameters provide valuable insights in designing socially inclusive workspaces, they require extensive datasets and cannot be expressed in EAWS-based force scores. A second approach assesses levels of muscular contractions as a function of the Maximal Voluntary Contraction (MVC), where onsets are detected by evaluating the signal's energy using the Teager–Kaiser Energy Operator (TKEO) [14,46]. Various protocols have been proposed to isolate muscular groups in isometric contractions [47,48].

Finally, IoT-based methodologies to evaluate the third EAWS section (i.e., Manual Material Handling) remain largely unexplored. Similar to the previous EAWS section, the reviewed literature presents MMH analysis based on conventional approaches and different ergonomic indices (e.g., NIOSH and EAWS) [49,50]. Benefitting from EAWS scores, [50] redesigns three workstations to lower MMH risks for employees. In this work, the digital evaluation of material handling is addressed using MOCAP and sEMG measurements [14,38,51]. Despite the mentioned enabling IoT technologies being capable of digitizing the first three EAWS sections, they fall short in segmenting working shifts into specific manual activities. Indeed, these sensors overlook the temporal dimension (e.g., repetition rates), which is a critical parameter in calculating EAWS scores as well. As a result, relating safety weaknesses in human-centric production processes to singular manual tasks would be more challenging.

To address this important limitation, RFID technology is introduced due to its significant capabilities in enhancing process traceability [52,53]. Recent solutions propose the use of smart gloves equipped with integrated and compact RFID-based antennas [54]. Plant supervisors can strategically deploy passive tags in key manufacturing areas (e.g., supermarkets and product bins) and on entities (e.g., tools and sub-assemblies) to identify OPIs throughout activity executions [14], including actions like component picking and tool usage.

The following bullet points list the main innovative contributions of this manuscript:

- **Digital EAWS evaluation:** Different IoT technologies automate the evaluation of the first three EAWS sections, namely Basic Postures, Action Forces, and Manual Material Handling. The measuring devices include a MOCAP network, a sEMG sensor, and an RFID-based smart glove (see Section 3.1). While the first two acquire workers' 3D body joints and upper limbs' muscular contractions, the RFID-based solution enables the detection of OPIs. The acquired data streams are fed into computational algorithms to evaluate the EAWS-informed KRIs (see Section 3.2).
- **EAWS-informed KRIs:** These metrics are derived from the EAWS score and are embedded into an ergonomic DSS. The proposed KRIs evaluate the safety-related weaknesses from different perspectives, providing decision-makers with privileged opportunities to redesign human-centric workplaces. Section 5 discusses their importance in analyzing the assembly of home furniture.

3. Digital architecture

This section details the developed digital architecture designed to enhance the physical resilience of Operators 5.0 in human-centric manufacturing systems (refer to Fig. 1). The acquisition layer integrates three enabling IoT technologies to automatically evaluate the Basic Postures, Action Forces, and Manual Material Handling sections of the EAWS screening tool. The RFID technology detects OPIs, while MOCAP cameras and sEMG wearables capture time-driven body joint positions and muscular contractions, respectively. Computational algorithms process these diverse data streams to perform task-driven assessments of the aforementioned EAWS sections. Consequently, an ergonomic DSS presents multidimensional KRIs to identify operator- and process-specific safety weaknesses. For instance, the Musculoskeletal Risk metric, in addition to assigning a global risk score for any manufacturing task, displays the time-dependent body angles for each human posture. This granular level of detail proves invaluable for industrial plant supervisors in initiating process modifications, such as assembly line re-balancing.

3.1. Enabling IoT technologies

As previously mentioned, three enabling IoT technologies collect process, physiological, and motion measurements: (i) the RFID smart glove, (ii) the sEMG data acquisition system, and (iii) the MOCAP camera network.

The RFID-based glove identifies OPIs by reading passive tags attached to tools and fasteners. The Radio Frequency reader uses the battery-powered PyScan device [55], which integrates the NXP MFRC63002 RFID transceiver and connects wirelessly to a server via Wi-Fi. The device sends the ID of each scanned RFID tag to the server using the Message Queuing Telemetry Transport (MQTT) protocol. On the server, the timestamp associated with the detection moment for each tag is recorded along with its ID and stored in an InfluxDB database.

The sEMG data acquisition system uses the BITalino evaluation kit [56], which incorporates the Atmega 328P microcontroller, the HC-6 Bluetooth transceiver, and the AD8232 instrumentation amplifier. For each sEMG channel, the AD8232 amplifies the provided signal; the signal is acquired by the 10-bit Successive Approximation Register Analog-to-Digital Converter (ADC) embedded in the microcontroller. The data acquisition board exhibits a Signal-to-Noise Ratio (SNR) of 55.72 dB, delivers an Effective Number Of Bits of 8.73 bits, and operates at a sampling rate of 1 kHz [56]. Acquired samples are streamed in real-time via Bluetooth to a gateway and transmitted to the server via Wi-Fi. On the server, each sEMG sample is stored with its acquisition timestamp. The monitored muscles include both the left and right biceps and forearms [23].

The MOCAP system consists of two Microsoft Azure Kinect devices [57] to mitigate acquisition errors in occlusion scenarios [14]. These devices are synchronized with each other using an audio cable. Each device embeds a 1-MP (MegaPixel) depth sensor with a variable field-of-view and a 12-MP RGB (Red, Green, Blue) video camera, operating at a frame rate of 15 fps. The MOCAP network is positioned in the manufacturing layout, synchronized through an absolute clock, and calibrated via a checkerboard pattern. Cameras are placed to maximize the coverage area and minimize potential sources of obstructions. Recordings from each device are processed frame by frame in a loop for identified bodies, to which specific IDs are assigned. Calculations for determining body joint positions start at the pelvis and extend to the ears, ensuring interrelationships using a global approach. The resulting 3D coordinates of body joints, along with associated confidence levels, are saved in separate output files, while timestamps are stored for each data stream.

The following computational algorithms detail how to fuse the video-based distributed measurements to obtain a reference worker representation (see Section 3.2.2). The recorded parameters, such as sEMG signals and body joint coordinates, undergo synchronization during the post-processing stage within the computational steps of OPIs (refer to Section 3.2.1). Following this synchronization, the EAWS index is digitally reconstructed by integrating physiological and process-related measurements (see Table 1).

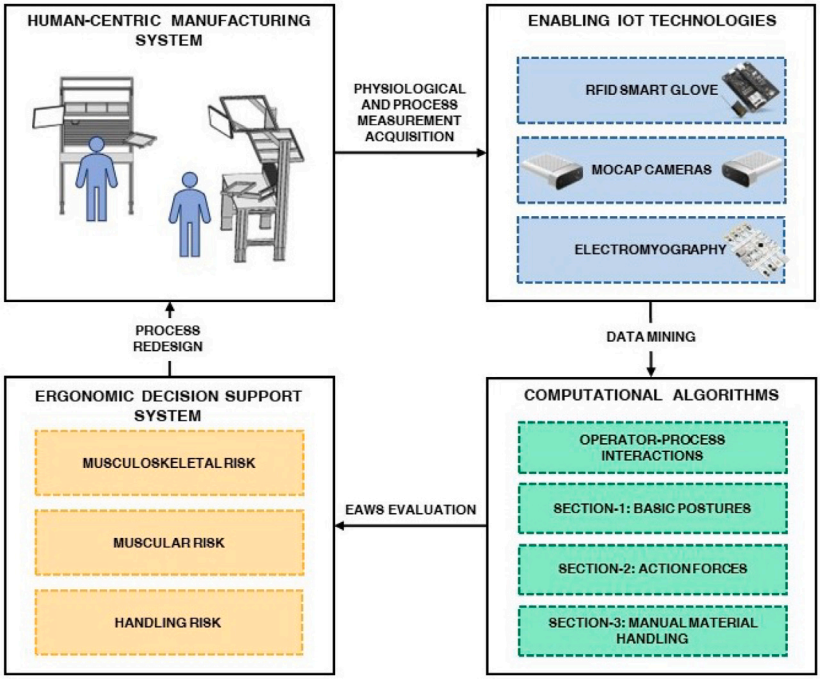

Fig. 1. Overview of the digital architecture for evaluating the EAWS.

Table 1
Role of enabling IoT technologies in digitizing the EAWS index.

EAWS Section	RFID	MOCAP	sEMG
Basic Postures	✔	✔	✘
Action Forces	✔	✘	✔
MMH	✔	✔	✔

3.2. Computational algorithms

Based on the discussed IoT technologies, this section outlines the computational algorithms for extracting value from the acquired data streams and digitizing the EAWS-driven sections. Despite the synchronous acquisition of physiological and process data, an initial computation utilizes RFID-based measurements to segment workers' activities and recognize tool usage (refer to Section 3.2.1). For each assembly task, a parallel set of computations is initiated to evaluate three sections of the EAWS: Basic Postures (Section 3.2.2), Action Forces (Section 3.2.3), and MMH (Section 3.2.4). While the first two assessments consider the MOCAP and sEMG data streams independently, the third section integrates the three IoT technologies to compute the KRIs for this ergonomic dimension (refer to Table 1). Finally, two Appendices ease the reading process of this methodology. While Appendix A summarizes the indices and parameters, Appendix B lists the body joints used to evaluate EAWS postures.

3.2.1. Operator-process interactions

This pre-processing step utilizes RFID-based data streams to identify OPIs and synchronize measurements from the other IoT technologies. Specifically, data are downloaded from a server through a Secure Shell (SSH) connection and divided into task- and tool-driven measurements.

Although the computational steps for mining value from data streams are fairly similar, the discussion starts with task recognition (see Algorithm 1). For assembly activities, time windows are reconstructed based on successive pickings of components, fasteners, or Work-In-Progress (WIP) products. This process depends highly on the manufacturing workflow and requires consideration of metadata. Therefore, it is crucial to deploy passive tags in strategic locations within the manufacturing system (e.g., supermarket trays). The RFID-based glove continuously reads passive tags' unique strings and associates the corresponding timestamps. AS_f and AT_f represent these parameters during the fth recording frame. AT_f and AT_{f+1} are temporally spaced by δ, the sampling rate of the RFID-based glove. It is reasonable to gather the same AS multiple times for consecutive frames whenever workers pick components from the activity-related bin. Based on these raw data, Algorithm 1 exploits two while loops to create a scan list for each ath activity of the assembly sequence (e.g., $Scan_a$).

Algorithm 1 Time-series algorithm to detect activity-oriented OPIs

Require: AT_f and AS_f $\forall f = 1, ..., F$
1: Initialize T_a and S_a as empty parameters
2: $f = 1$
3: $a = 0$
4: **while** $f \leq F$ **do**
5: $a = a + 1$
6: **while** $(AT_{f+1} - AT_f \leq \delta)$ **and** $(AS_{f+1} = AS_f)$ **do**
7: **Add** AT_{f+1} to the list $Scan_a$
8: $f = f + 1$
9: **end while**
10: $T_a = min(Scan_a)$
11: $S_a = AS_f$
12: **end while**
13: **return** T_a and S_a, $\forall a = 1, ..., A$

In particular, AT_{f+1} values are continuously added to $Scan_a$ if their temporal difference with the current timeframe is at most equal to δ. To avoid mixing assembly activities, an additional check ensures that AS_{f+1} and AS_f agree (see while statement in line 6). Once the algorithm exits the inner while loop, it computes the starting time of the ath activity and associates the respective tag string (see lines 10 and 11). It is worth noting that T_{a+1} represents both the starting and ending time for the $(a + 1)$th and ath assembly activities, respectively. Therefore, the duration of the ath assembly activity is given by the difference between T_{a+1} and T_a.

The automatic detection of tool usage follows similar computational steps to those discussed in Algorithm 1. Assuming each tool is embedded with a passive tag, $TS_{f'}$ and $TT_{f'}$ represent the unique tool strings and the associated timestamps, respectively. These time-driven

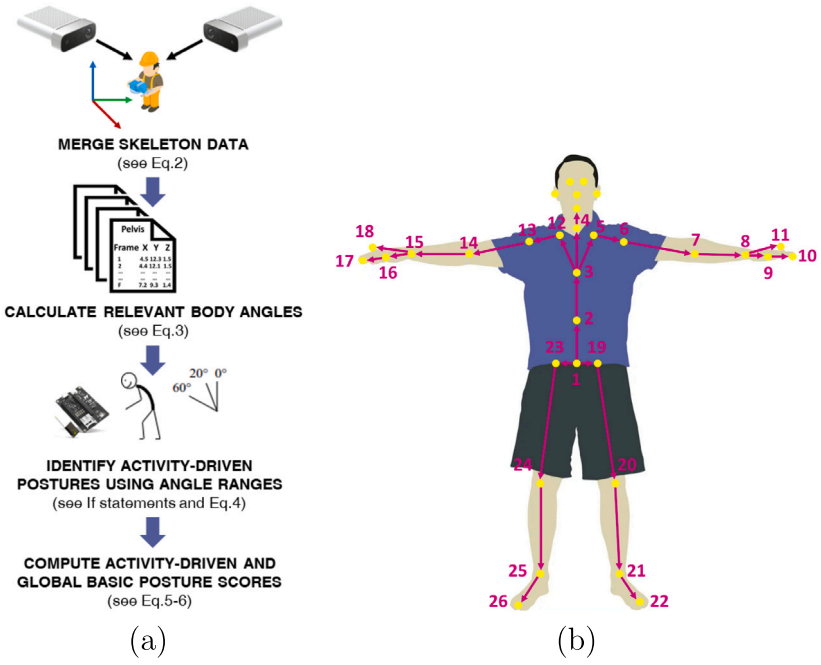

Fig. 2. (a) Flow diagram for musculoskeletal risk assessment; (b) Human body joints captured by the Microsoft Azure Kinect cameras.

parameters are processed by the same two while loops. However, these OPIs derive different parameters from $Scan_t$ when the algorithm breaks the inner loop. Each tth tool usage is distinguished by a starting time (i.e., $TTstart_t$), end time (i.e., $TTend_t$), and tool string (i.e., S_t). While $TTstart_t$ and $TTend_t$ are equal to the earliest and latest $TT_{f'}$ values belonging to $Scan_t$, S_t corresponds to the tag string currently processed by the inner loop (i.e., $TS_{f'}$). To increase the consistency of the detected tool-driven OPIs, two additional hyperparameters can be introduced to mitigate the intrinsic uncertainty of human factors. First, tool usages with durations shorter than α can be discarded. Second, consecutive tool-driven OPIs are merged if the following condition is met:

$$TTstart_{t+1} - TTend_t \leq \tau; \text{ where } S_t = S_{t+1} \tag{1}$$

Benefiting from the evaluated activity- and tool-oriented OPIs, a parallel stream of computations is triggered to calculate the EAWS-based index. The algorithm selects the time-specific measurements from the MOCAP cameras and the sEMG wearable for each ath activity of the assembly sequence. The following sections quantitatively describe the computational steps to digitize the Basic Postures (Section 3.2.2), Action Forces (Section 3.2.3), and MMH (Section 3.2.4) EAWS sections.

3.2.2. Section 1 - Basic postures

This first algorithm branch automatically identifies time-dependent body angles and the related human postures to calculate the Basic Postures-informed KRIs, based on the computational steps described in Fig. 2(a). Following the initialization of the MOCAP camera network according to Section 3.1, the first computational step performs human skeleton fusion using the 3D coordinates of body joints (i.e., $Pos^c_{b,k}$) and the related measurement confidence levels (i.e., $CL^c_{b,k}$). These parameters are indexed by b, k, and c, representing the body joint, the recording frame, and the Kinect camera, respectively. The algorithm selects body joint coordinates with the highest confidence level as follows:

$$Pos_{b,k} = \arg\max_{b,c}\{CL^c_{b,k}\};\ \forall\, b = 1,\dots,B \text{ and } k = 1,\dots,K \text{ and } c = 1,2 \tag{2}$$

Subsequently, the returned body joint positions are indexed to the detected assembly activities (i.e., $a = 1,\dots,A$) based on the computed OPIs (see Section 3.2.1). To facilitate the assessment of relevant body angles, the human skeleton is recreated using the hierarchical structure depicted in Fig. 2(b), where the pelvis (i.e., Joint 1) represents the root node. The EAWS screening tool defines several human movements from lumbar extension to arm positions; therefore, Appendix B lists the body joint groups considered to identify each posture. Based on this, the algorithm traverses the body tree with a depth-first order iterator to calculate two vectors. First, a 3D vector is computed between each joint and its parent (e.g., Joint 1 is the parent of Joint 2). Second, the program creates G vectorial structures of body joint groups (i.e., $V^a_{g,k}$). In particular, $V^a_{1,k}$ represents the back vector between joints ranging from 1 to 4. The vector of the right leg, $V^a_{2,k}$, is formed by considering the body joints 1, 23, 24, and 25. Therefore, the angle between the worker's back and the right leg is given as follows, where g and g' are equal to 1 and 2, respectively:

$$\Theta^a_{g-g',k} = \arccos\left(\frac{\mathbf{V^a_{g,k}} \cdot \mathbf{V^a_{g',k}}}{\|\mathbf{V^a_{g,k}}\|\|\mathbf{V^a_{g',k}}\|}\right);\ \forall k = 1,\dots,K \text{ and } g, g' \in G \tag{3}$$

It is worth noting that this angle is computed for all postures and body joint groups in Table B.3 of Appendix B, in addition to each kth recording frame of the MOCAP-based network. However, $\Theta^a_{1-2,k}$ is not sufficient to adequately classify back inclinations. $\Theta^a_{1-3,k}$ is computed following the same procedure, where g equal to 3 indexes the left leg. Based on Table B.3, the involved joint numbers are 1, 19, 20, and 21.

Using $\Theta^a_{1-2,k}$ and $\Theta^a_{1-3,k}$, the algorithm scans all timeframes and performs activity-driven posture (i.e., $p = 1,\dots,P$) recognition through the following if statements:

- **If** $\Theta^a_{1-2,k}$ and $\Theta^a_{1-3,k} < 20° \Rightarrow$ **Standing** (i.e., $p = 2$)
- **If** $20° \leq (\Theta^a_{1-2,k}$ and $\Theta^a_{1-3,k}) \leq 60° \Rightarrow$ **Low Bending** (i.e., $p = 3$)
- **If** $\Theta^a_{1-2,k}$ or $\Theta^a_{1-3,k} > 60° \Rightarrow$ **High Bending** (i.e., $p = 4$)

Based on these statements, a duration is automatically assessed for each pth EAWS posture and ath assembly activity (i.e., D^a_p). $Tstart^a_p$ and $Tend^a_p$ represent the starting and ending timestamps, respectively. Subsequently, D^a_p is mapped into risk scores (i.e., $PScore^a_p$) following the EAWS guidelines. For instance, a low bending duration of 16 s (i.e., D^a_3) corresponds to a $PScore^a_p$ equal to 12. It should be noted that some movements are mutually exclusive (e.g., standing, bending,

and strong bending), while other postures can be assumed simultaneously (e.g., standing and trunk rotation). Additionally, posture-related parameters are indexed to r to indicate the temporal occurrence of the pth posture in a (i.e., $D^a_{p,r}$ and $PScore^a_{p,r}$). The last processing step in activity-driven posture identification mitigates the acquisition noise of the MOCAP-based network and the intrinsic motion uncertainty of human workers. For example, consider three consecutive postures with known durations $D^a_{p,r-1}$, $D^a_{p',r}$, and $D^a_{p,r+1}$. The algorithm considers the two pth postures as a single event if the following condition is verified.

$$D^a_{p+1,r} \leq \beta \tag{4}$$

where β represents the minimum duration to hold an EAWS-driven posture. Trivially, merging postures requires updating all related parameters. The resulting Activity-Driven and Global Action Forces Scores are computed using Eqs. (5) and (6), respectively:

$$ADBPS^a = \sum_{r=1}^{R}\sum_{p=1}^{P} PScore^a_{p,r};\ \forall p, r \in a \tag{5}$$

$$GBPS = \frac{\sum_{a=1}^{A} ADBPS^a}{A} \tag{6}$$

3.2.3. Section 2 - Action forces

This algorithmic branch computes the second section of the EAWS index, focusing on the exerted forces of upper limbs (i.e., biceps and radial flexors) during task executions. Traditionally, muscular strength is defined as a subject's capability to apply a force over a given time window. The applied force is a complex phenomenon involving interactions with muscle fibers and the central nervous system [58]. Despite this data usually being acquired by dynamometers, [59] demonstrates, based on limits of agreements, that sEMG data streams are a reliable measure to detect changes in muscle strength and muscle activity. Therefore, this algorithm leverages sEMG-based signals to assess Voluntary Contractions (%VC) as a function of MVC in workers' upper limbs and then associates these to action force scores defined by the EAWS screening tool [24]. This approach facilitates the development of this section by neglecting assumed postures.

Before evaluating muscular-driven VC and the related KRIs, the algorithm needs to be initialized for each worker according to the right path of Fig. 3. This initialization involves N sEMG acquisitions, capturing muscular datasets during resting and maximal isometric contraction scenarios. While the initial data streams help determine acquisition noise for each channel (i.e., $noise_m$), the muscle-driven MVC_m (i.e., where $m = 1, \dots, 4$) is computed based on the second set of recordings. The evaluated VC_m is normalized using the corresponding MVC_m, and thus this parameter is represented as % VC_m. Muscular measurements undergo denoising and conditioning through a three-step approach:

1. **Wavelet Package Decomposition (WPD)**: It splits signals into high and low-frequency coefficients (i.e., detail and approximation, respectively). The Daubechies 45 orthogonal mother wavelet is employed, known for its efficacy in handling sEMG data [60]. After decomposition, the sEMG information is recomposed by summing the approximation coefficient of the last order with the detailed ones.
2. **TKEO**: It enhances SNR and onset muscle activation detection [23].
3. 4**th-order low-pass Butterworth filter**: It obtains the envelope, removing frequency components at twice the signal bandwidth.

This three-step approach is applied to incoming sEMG data streams and is not repeated when analyzing the left part of the flow diagram in Fig. 3. The algorithm computes acquisition $noise_m$ and MVC_m. The acquisition noise is approximated to three times the standard deviation of the signal in resting scenarios for any mth active channel or muscle. Multiple acquisitions (i.e., $noise^n_m$, where $n = 1, \dots, N$) are

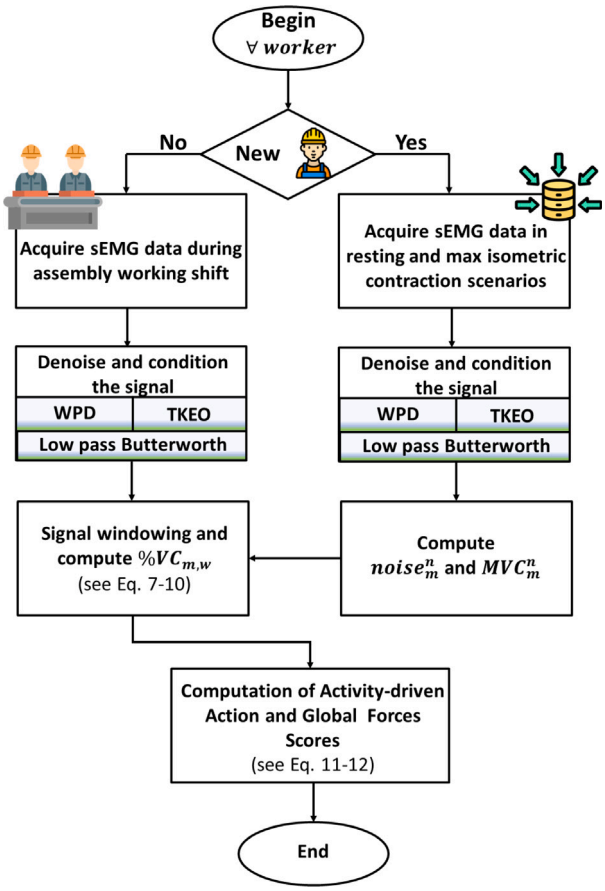

Fig. 3. Flow diagram for evaluating muscular risk.

recommended to enhance the metrological reliability of this parameter. The resulting $noise_m$ is equal to the mean of all acquisitions. MVC^n_m is obtained by performing for a variable duration (i.e., D^n_m) isometric contractions of the biceps brachii and radial flexors. Similarly, MVC_m and D_m are obtained by averaging the maximal voluntary contraction and duration of each nth recording and mth sEMG channel, respectively. It is crucial to note that these parameters highly depend on operators' physical features, varying within the workforce and even between subjects' sides.

Following this worker and muscle-specific initialization procedure, the algorithm is ready to analyze sEMG measurements acquired during industrial working cycles as depicted by the left flow part in Fig. 3. In the following, sEMG data streams are denoted as $x_{i,m}$, where i represents the acquisition frame of the BITalino board. The algorithm performs a signal windowing step to evaluate the % VC_m. In particular, it defines muscle-specific overlapping sliding windows with duration (i.e., $Wdur_m$) and overlap (i.e., $over_m$) equal to D_m and $D_m/2$, respectively. Within each wth sliding window, the absolute magnitude of muscular contractions (i.e., $AMMC_{m,w}$) and related duration (i.e., $DMMC_{m,w}$) are computed by thresholding the signal energy as follows:

$$AMMC_{m,w} = \sum_{i=1}^{I} f(x_{i,m});\ \forall\ x_i \geq thr_m \text{ and } m = 1, \dots, 4 \tag{7}$$

$$DMMC_{m,w} = \sum_{j=1}^{J} (x_{j+1,m} - x_{j,m});\ \forall\ x_{j,m} = thr_m \text{ and } m = 1, \dots, 4 \tag{8}$$

where thr_m is equal to $noise_m$. As a result, the muscular activation and the $\%VC$ for each muscle and window are computed using the

following equations:

$$MA_{m,w} = \frac{AMMS_{m,w}}{DMMC_{m,w}};\ \forall\ w = 1,\dots,W \text{ and } m = 1,\dots,4 \quad (9)$$

$$\%VC_{m,w} = \frac{MA_{m,w}}{MVC_{m}};\ \forall\ w = 1,\dots,W \text{ and } m = 1,\dots,4 \quad (10)$$

It is worth noting that muscular activations might be dynamic and their distribution may be sparse among muscular groups and assembly tasks. Scaling this computational approach for each ath activity in the assembly sequence, the previously mentioned parameters can be indexed also to a. For instance, $MA^{a}_{m,w}$ represents the muscular activation of the mth recording channel during the wth window of the ath assembly task. Trivially, multiple w windows can belong to the same ath assembly activity. Before computing the KRIs for the Action Forces section, $DMMC^{a}_{m,w}$ and $\%VC^{a}_{m,w}$ are mapped into EAWS scores based on the ergonomic tool's tabular values [24]. For instance, $\%VC^{a}_{m,w}$ equal to 17% provides an intensity score (i.e., $FScore^{a}_{m,w}$) equal to 6 points. Similarly, a duration score (i.e., $DFScore^{a}_{m,w}$) equal to 1.5 points is associated with a $DMMC^{a}_{m,w}$ of 10 seconds. The resulting Activity-Driven score is computed using the following equation:

$$ADAFS^{a}_{m} = \frac{\sum_{w=1}^{W} FScore^{a}_{m,w} \times DFScore^{a}_{m,w}}{W};\ \forall w \in a \quad (11)$$

The score for the ath activity (e.g., $ADAFS^{a}$) is equal to the greatest value of $ADAFS^{a}_{m}$. Based on $ADAFS^{a}$, the Global Action Forces score is given as follows:

$$GAFS = \frac{\sum_{a=1}^{A} ADAFS^{a}}{A} \quad (12)$$

The next section integrates posture-dependent information and muscular activities to evaluate the ergonomic risk in handling heavy loads.

3.2.4. Section 3 - Manual material handling

This third algorithm branch detects MMH events and evaluates the physical resilience of workers through Handling KRIs. To achieve this purpose, the enabling IoT technologies measurements and process metadata are leveraged as conceptually depicted in Fig. 4. Firstly, the operator-centric manufacturing sequence is divided into A assembly activities through the RFID-based automatic recognition of OPIs (refer to Algorithm 1 in Section 3.2.1). In particular, this activity segmentation is performed with T_a of detected tasks. The algorithm then iterates over assembly tasks based on x_a. This binary variable is equal to 1 if the associated task processes a WIP weighing 3 kg or more; otherwise, it is equal to 0 [24]. The weight is process metadata retrieved from the use case's information systems. Within activities having x_a equal to 1, an additional windowing step is executed (see Fig. 4). The target is to exclude tool usage time windows using $TTstart_t$ and $TTend_t$. The complementary time intervals (i.e., the blue-colored ones) represent potentially relevant MMH events. For each event, overlapping sliding windows segment the sEMG-based data streams to compute $\%VC_{m,w}$. Significant MMH windows are distinguished by $\%VC_{m,w}$ greater than a threshold (i.e., γ) for at least one muscular group. Therefore, $Tstart^{a}_{v}$ and $Tend^{a}_{v}$ represent the starting and ending timestamps of the vth relevant MMH event during the ath assembly activity.

Four different postures need to be detected within these windows. These include trunk upright, little trunk bending, deep trunk bending, and asymmetric movements or kneeling. In particular, a score risk (i.e., $MMHPS^{a}_{s,v}$) is associated with these MMH postures (i.e., $s = 1,\dots,4$). For instance, while carrying a load in the trunk upright position ($s = 1$) scores 1 posture point, in the deep trunk bending position ($s = 3$), it scores 4 posture points. It is worth noting that multiple postures may occur in the same vth relevant MMH event. The resulting posture score of that MMH event (i.e., $MMHPS^{a}_{v}$) is equal to the greatest value of all postures. The second risk metric targets the duration of the entire MMH event (i.e., D^{a}_{v}), derived from $Tstart^{a}_{v}$ and $Tend^{a}_{v}$. D^{a}_{v} is multiplied by the total duration of the work shift, typically set at 480 minutes, and then divided by the duration of the specific manufacturing task under consideration, which is assumed to repeat cyclically. The resulting frequency F_v is mapped into $MMHFS_v$ following the EAWS tabular values. For instance, F^{a}_{v} equal to 5 provides an $MMHFS_v$ of 1 point. Finally, WS^{a} represents the risk score associated with the handled weight during the ath assembly activity with x_a equal to 1. The EAWS lists different risk scores for carried loads based on the worker's gender. This metadata is not considered to ensure the privacy of final users and facilitate the architecture adoption in unionized industries. Therefore, carried load risk scores always refer to the female gender, which is distinguished by higher values. For instance, lifting a 5 kg weight corresponds to 1.5 load points (i.e., WS^{a}). Finally, the Activity-driven and Global MMH scores are computed using:

$$ADMMHS^{a} = \frac{\sum_{v'=1}^{V}(MMHPS^{a}_{v} + WS^{a}) \times MMHFS_{v}}{V};\ \forall v' \in a \quad (13)$$

$$GMMHS = \frac{\sum_{a=1}^{A} ADMMHS^{a}}{A} \quad (14)$$

To conclude this high-detailed and quantitative section, Fig. 5, combined with Appendices A and B, highlights the key steps to calculate three EAWS sections. After the data acquisition of OPIs, workers' body joints, and upper limbs' muscular contractions, the computational algorithms are triggered to extract EAWS-informed KRIs. The first processing step targets the segmentation of assembly tasks and tool usage in human-centric manufacturing systems (see Algorithm 1). The activity recognition is a strategic output of the algorithm since it enables the development of task-specific risk metrics. Subsequently, three parallel computational streams are triggered to digitize the following EAWS sections:

- **Section 1 - Basic Postures:** After reconstructing the worker's skeleton using MOCAP cameras' confidence levels (see Eq. (2)), this algorithm branch iterates over the body joints to create muscular group vectors and then evaluate angles among them (see Eq. (3)). Appendix B lists the body joint groups to successfully identify relevant body angles. These parameters are exploited to detect EAWS-driven postures. For example, Section 3.2.2 presents three If-statements to identify *standing*, *bent forward*, and *strongly bent forward* based on angles formed between the back and the legs. Finally, Eq. (5) and (6) formalize the Activity-driven and Global Basic Posture KRIs.
- **Section 2 - Action Forces:** This algorithm branch leverages sEMG-based upper limbs' contractions to evaluate exerted forces during task executions. Following a pre-processing step that acquires worker-specific hyperparameters such as $noise_m$ and MVC_m, sEMG-based data streams are leveraged by overlapping windows. For each muscle-driven wth window, the program extracts $\%VC_{m,w}$ in four different steps (see from Eq. (7) to Eq. (10)). Finally, EAWS scores of relative voluntary contractions and related durations are leveraged to compute the Activity-driven and Global Action Forces KRIs (i.e., Eq. (11) and (12)).
- **Section 3 - Manual Material Handling:** This third computational stream evaluates workers' risk during handling operations. First, the algorithm iterates over assembly activities with products weighing more than 3 kg and identifies potentially relevant MMH events by removing tool usage time windows (see Fig. 4). The mentioned events are labeled as relevant if at least one muscular $\%VC_{m,w}$ is greater than a threshold. It is worth noting that the calculation of relative voluntary contractions follows the same procedure described to digitize the previous EAWS section. Within relevant MMH events, the algorithm assigns EAWS scores to the assumed posture (i.e., $MMHPS^{a}_{v}$), the frequency of the vth event (i.e., $MMHFS^{a}_{v}$), and the load weight (i.e., WS^{a}). Based on these parameters, the Activity-Driven and Global Manual Material Handling KRIs (i.e., Eq. (13) and (14)) are computed.

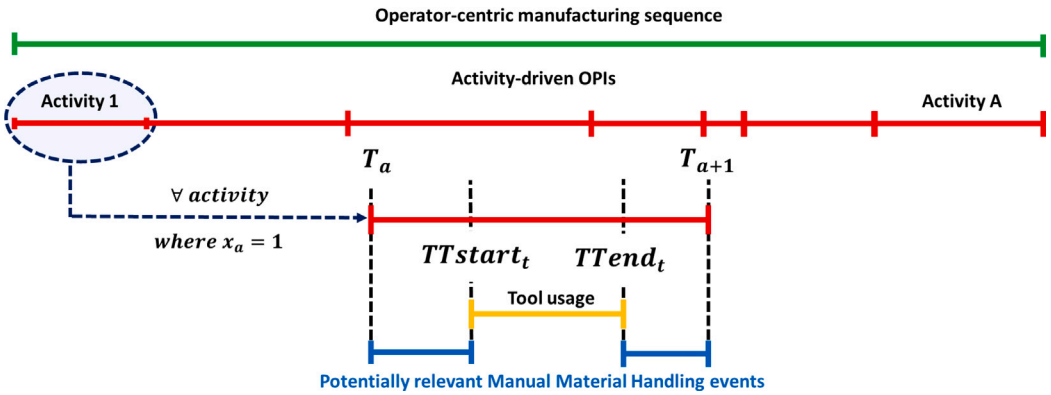

Fig. 4. Time-driven approach to detect potentially relevant MMH events.

Table 2
Example of time-dependent assembly activities for a monitored worker.

Task ID	Start	End	Tool	Tool usage [s]	Basic posture	Action forces	MMH	Whole body
Task 1	14:31:23	14:37:00	Screwdriver	215.4	37	22.9	0	37
Task 2	14:42:28	14:43:59	Manual	91.0	35	127.5	0	127.5
Task 3	14:57:40	14:58:18	Manual	38.3	29	51	2.2	51
...	...	...	...	...	...	...	...	
Task N	15:12:35	15:13:56	Hammer	21.1	22	0	0	22

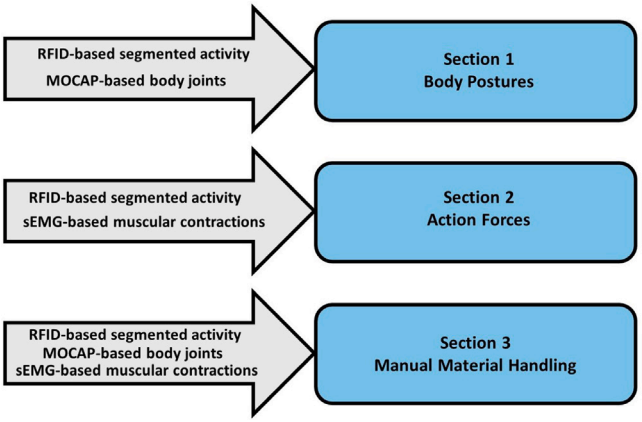

Fig. 5. Data model of the proposed digital architecture.

3.3. Ergonomic decision support system

Benefiting from the discussed computational steps to digitize the EAWS ergonomic tool, Table 2 summarizes how time-dependent assembly activities can be structured for a given working time window. The first five columns are generated by automatically identifying OPIs. Task segmentation is facilitated by RFID passive tags placed on components and WIP products, while continuous readings of tool tags provide information on their activity-based usage. A task is trivially labeled as *Manual* when no tools are detected during its duration. The columns for Basic Posture, Action Forces, and MMH are developed based on the algorithms described from Section 3.2.2 to Section 3.2.4. Finally, the last field (i.e., Whole Body) integrates the EAWS scores from the previous three categories to yield an aggregate risk metric. EAWS rules dictate that each manufacturing activity should be associated with just one score: a task can be identified as risky either due to the postures, the forces exerted, or the load lifted by the operator [24]. Therefore, the Whole Body Activity-Driven Score is determined from the highest score among the three. The Global Whole Body Score, on the other hand, is the average of the Whole Body Activity-Driven Scores.

This EAWS-based scoring system is crucial for identifying operator-driven safety weaknesses in manufacturing systems. However, it falls short of revealing the root causes of potentially hazardous events affecting workers' physical resilience. For instance, a high Basic Posture score may be driven either by bending postures or by the arms' positions above shoulder level; depending on the case, there are different considerations to make regarding the musculoskeletal risk to which the operator is subjected. Time-driven insights are also overlooked, and underestimating the effect of posture duration can lead to sub-optimal workplace redesign approaches and strategies. These limitations also apply to Action Forces and MMH scores. For example, the latter fails to highlight the most exposed muscles and their % VC during task executions. To address this gap, callback functions are developed to complement the discussed scores with additional KRIs. These KRIs are grouped into three different levels of detail, as follows:

- **Musculoskeletal**: Global Basic Posture Score; Activity-Driven Basic Posture Score; Fine-Grained Posture Score; Body Angle Evolution.
- **Muscular**: Global Action Forces Score; Activity-Driven Action Forces Score; Muscle-Specific and Time-Oriented % VC; Muscle-Specific Action Forces Score.
- **Handling**: Global MMH Score; Activity-Driven MMH Score; Activity-Driven Load Data; Muscle-Specific and Time-Oriented % VC; Postures Time in MMH Windows.

The effectiveness of this digital architecture in automating the EAWS assessment is substantiated in the industrial-like pilot environment described in Section 4. Subsequently, Section 5 delves into the managerial implications of monitoring workers' physical resilience through the proposed multi-dimensional KRIs.

4. Case study

An extensive experimental campaign was conducted in the industrial-related pilot environment depicted in Fig. 6 to validate the IoT-based digital architecture. The objective is to automatically evaluate the operator-centric EAWS index and the related KRIs during the assembly of a drawer at an industrial-like workstation. The selected piece of home furniture has the following dimensions: 67 cm × 69 cm × 39 cm (i.e., H × L × W). The assembly sequence involves 22 distinct tasks; for

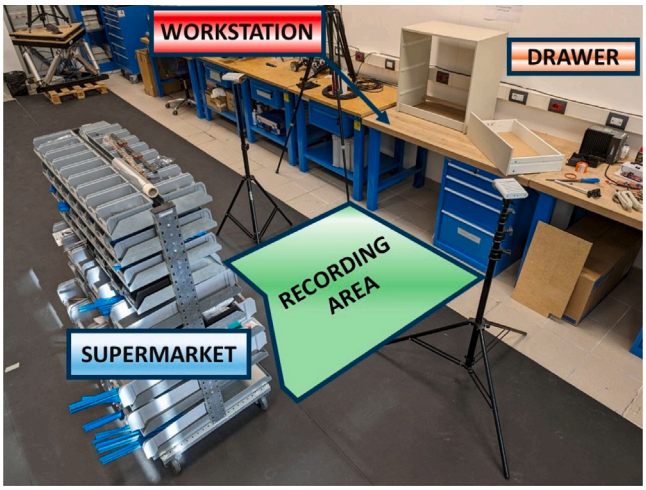

Fig. 6. Industrial-like pilot environment.

a detailed explanation of the process, interested readers are invited to refer to Appendix C. Operators perform the sequence using four manual tools: a hammer, a Phillips screwdriver, a slotted screwdriver, and a hexagonal Allen key. The human factor is digitized through the set of IoT technologies discussed in Section 3.1. The monitored operator wears an RFID smart glove to automatically detect OPIs (see Fig. 7). Assembly tasks and tool usage are automatically recognized based on components (e.g., fasteners) and tools retrieved from the supermarket and the workstation, thanks to RFID tagging in the pilot environment. Passive tags are placed in these storage locations, enabling the recognition of fine components picking and facilitating the activity segmentation process in the assembly sequence. Tools are also passively tagged to track their usage. For instance, the assembly process begins with the operator interacting with screw tags, which initiates the first activity. Following the predefined sequence, the worker uses a Phillips screwdriver to attach plastic plates onto drawer boards. Throughout this task, the RFID antenna inside the smart glove continuously scans the tool's code as long as it remains in the operator's hand. The activity concludes as the operator picks the next components required in the assembly sequence.

The RFID datasets stored in InfluxDB are imported into MATLAB and temporally synchronized with the other measurements. The MOCAP videos are converted to 3D human body joints using a C# script, while the 4-channel sEMG data streams are acquired using a Python script and imported into MATLAB in CSV format. To limit potential body joint occlusion that may affect EAWS scores [14], the MOCAP network consists of two cameras placed to the sides of the recording area (see Fig. 6).

Concerning sEMG data, Ag–AgCl disc-type disposable electrodes are used to record muscular contractions. Each BITalino channel is connected to a cable that splits into three ends for electrode attachments. The electrodes are carefully positioned on relevant muscle groups on the operator's upper limbs. As illustrated in Fig. 7, they are divided equally on the biceps and radial flexors of each body side.

Based on the extensive discussion of the algorithms reported in Section 3.2, the following part validates this digital architecture, demonstrating that the KRIs for Basic Postures, Action Forces, and MMH offer valuable insights for assessing the well-being of operators in human-centric manufacturing systems, according to Industry 5.0 pillars.

5. Results and discussions

The digital architecture proposed for assessing the physical resilience of manufacturing operators undergoes validation during the

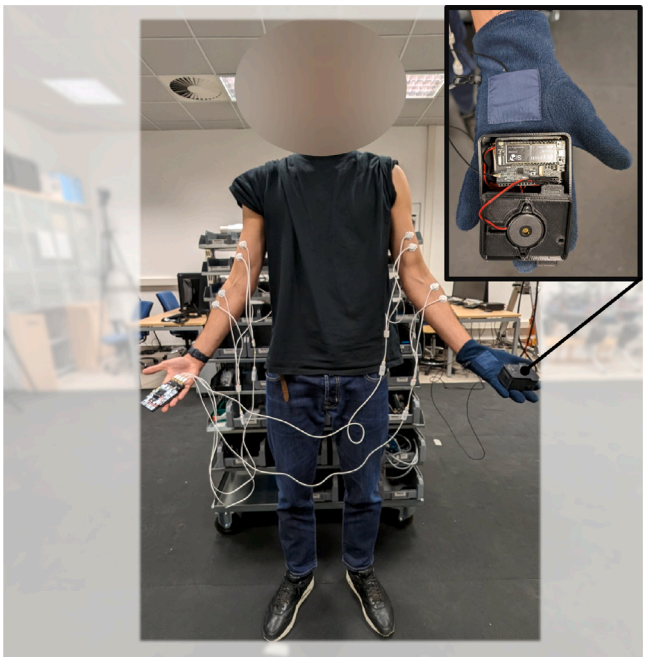

Fig. 7. The subject is wearing the RFID smart glove on the left hand (with a detailed view of the Pyscan board in the inset) and the BITalino electrodes positioned on the upper limb muscles.

assembly of the home furniture drawer described in Section 4. The example sequence presented in this part, which lasts 51.7 min, is decomposed into 22 assembly tasks by the automatic detection of RFID-driven OPIs. In Fig. 8, which shows this time-dependent subdivision, also including tool usage, some of the activities are repeated more than once. A detailed description of the task sequence can be found in Appendix C. This process-oriented insight provides two significant managerial implications. On the one hand, the architecture identifies the maximum, minimum, and average duration of assembly tasks. For instance, while one of the *Fixing Drawers* activities presents the longest execution time of 615.0 s, which involves the use of a slotted screwdriver for 61.3 s, the fastest assembly activity is one of the *Mounting White Caps*, which lasts 38.3 s. This information is relevant for identifying manufacturing weaknesses since task duration can be compared with historical data. In this regard, discussions with employees may reveal hazardous ergonomic scenarios. On the other hand, the architecture provides valuable information on tool usage. For example, in this assembly sequence, more than a third of the tasks are executed without tools. While the hexagonal Allen key is the least utilized tool, accounting for 9% of the total time of the process, the Phillips screwdriver is the most employed tool, reaching 23%. These insights are important in monitoring multiple workstations for a given manufacturing sequence. Indeed, utilization ratios can justify the economic initiative of purchasing additional tools to avoid potential bottlenecks.

Concerning the operator's ergonomic aspects, the digital architecture firstly returns the overall EAWS score. Fig. 9(a) highlights the Global Whole Body Score of 51.03 points, indicating a high-risk level. However, this initial ergonomic insight fails to pinpoint the most hazardous EAWS scores for the health of the monitored worker. Fig. 9(b) fills this gap by outlining the Global Section-Driven Scores, which include the Global Basic Posture score, the Global Action Forces Score, and the Global MMH Score, comparing them with the maximum section points totaled by the different assembly tasks. This insight, which is strategic to prioritize areas of improvement in the manufacturing system design, does not detail the riskiest tasks in the assembly sequence nor their worrisome parameters. Without this information, production

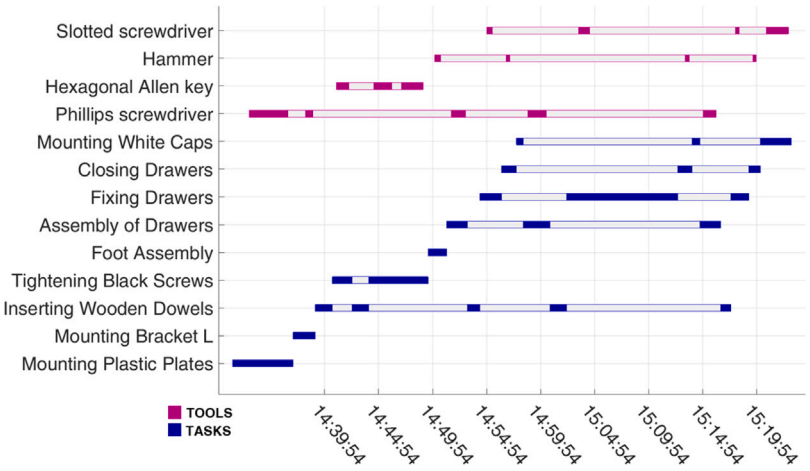

Fig. 8. The segmented manufacturing sequence, denoted as OPIs, along with tool usage: some of the 22 blue tasks are repeated over time, and each of the 4 violet tools is utilized multiple times.

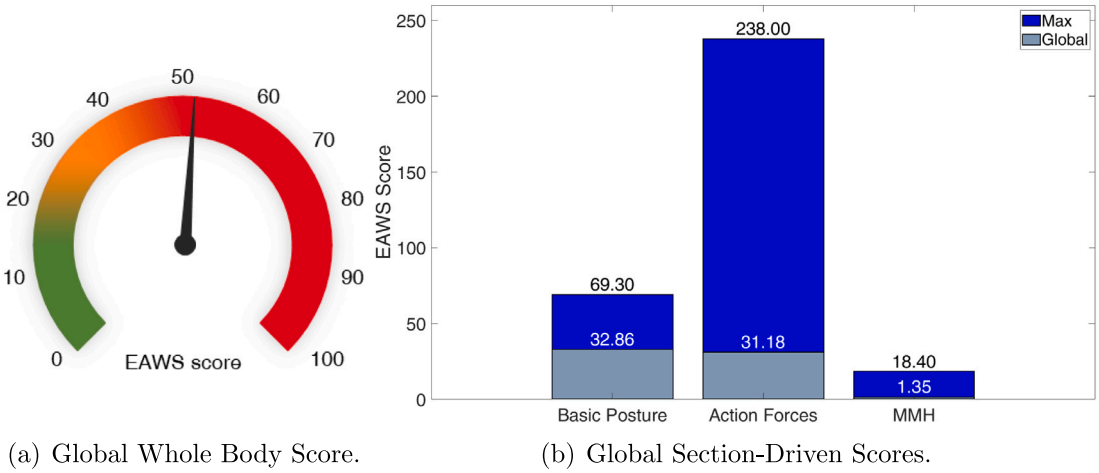

(a) Global Whole Body Score. (b) Global Section-Driven Scores.

Fig. 9. Preliminary insights into operator-centric physical resilience.

supervisors have no valid basis to reconfigure the workstation design or the assembly process. To avoid such a notable limitation, the following sections discuss the effectiveness of monitoring assembly sequences through the proposed KRIs and demonstrate the benefits of digitizing the EAWS index to increase the visibility of ergonomic weaknesses and safeguard the physical resilience of manufacturing operators.

5.1. Muscoloskeletal risk

Four postures significantly contribute to the Global Basic Posture Score, totaling 32.8 out of 69.3 EAWS points (refer to Fig. 9(b)). Specifically, these postures involve two levels of lumbar extension and asymmetric movements. While standing and bending scenarios account for 21.4% and 64.3% of the total score, the remaining 14% is linked to trunk rotation and far-reach movements, with 3 and 1 points assigned to them, respectively. Although this score suggests a moderate risk according to the EAWS index [24], it fails to highlight the most critical tasks in the musculoskeletal dimension. Leveraging RFID-enabled OPIs, Fig. 10 displays the Activity-Driven Posture Score in the time domain. It is evident that most of the assembly task scores fall within the medium-risk category (i.e., the range between 25 and 50 EAWS points), while 2 tasks stand out with scores exceeding 50 points, indicating high ergonomic risk. In effectively redesigning the manufacturing process, plant supervisors should prioritize the analysis of the most concerning tasks from a musculoskeletal perspective. For

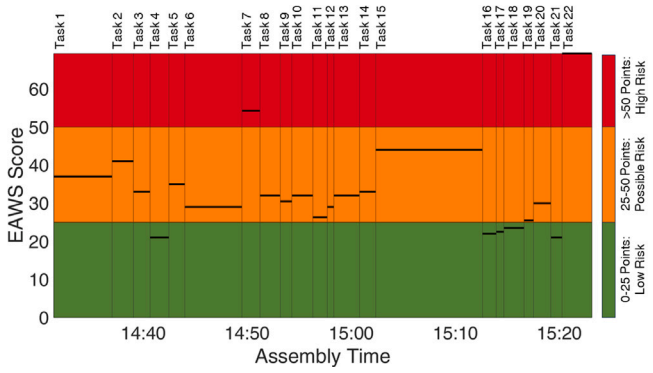

Fig. 10. Activity-Driven Basic Posture Score: the sequence of tasks and the associated EAWS risk levels are reported.

instance, the last assembly activity (i.e., *Mounting White Caps*) records the highest score, contributing 69.3 EAWS points over 171.7 s.

In addition to enhancing visibility into operator and activity-driven musculoskeletal risk, pinpointing the most impactful postures on each task score is strategic. Therefore, Fig. 11 depicts the Fine-Grained Posture Score for every movement performed by the operator during the last assembly activity: light and dark blue bars represent actual

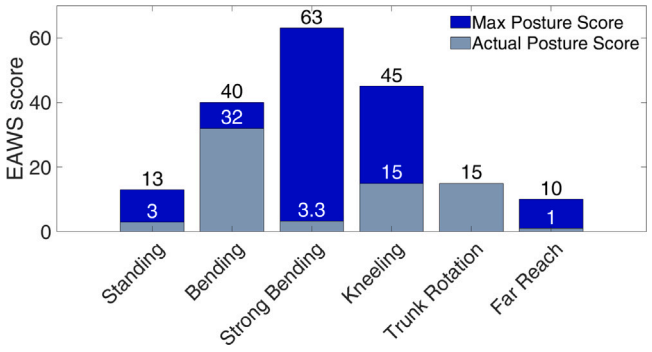

Fig. 11. Fine-Grained Posture Score: the actual (i.e., measured) and maximum achievable scores according to the EAWS database are reported for the pertinent postures of task #22.

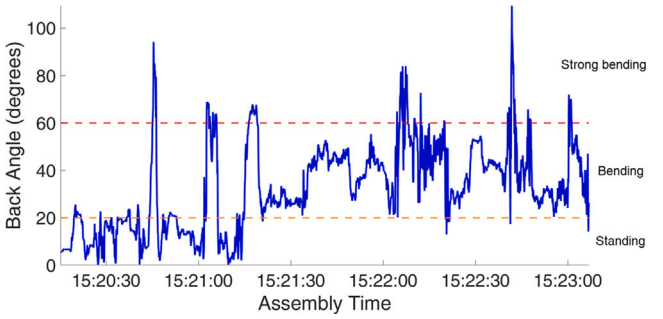

Fig. 12. Body Angle Evolution: the lumbar extension angle for task #22 is monitored. Postures are identified based on the angle's value over time: *standing* if the angle is less than 20°, *bending* if the angle is between 20° and 60°, and *strong bending* if the angle exceeds 60°. To ensure posture recognition accuracy, the algorithm corrects fluctuations by requiring the angle to remain within the same range for a certain number of consecutive frames.

(i.e., measured) and maximum EAWS scores, respectively. This task involves three main steps: (a) Retrieve the two previously assembled drawers from the adjacent worktable and place them inside the dresser, (b) Secure all the drawers using a slotted screwdriver, and (c) Insert the last drawer into the dresser. For further details, refer to Appendix C. This scenario may have critical implications for the physical resilience of workers since it might trigger potentially relevant bending postures (see Fig. 11) or burden the muscular activation of the upper limbs; the second implication will be better highlighted later.

The fine-grained KRI outlines that the bending and trunk rotation postures are the most critical movements, accounting together for 47 EAWS points. However, this risk metric falls short of suggesting the most appropriate operator-centric process reconfiguration approaches. Hazardous musculoskeletal scenarios may be driven by extremely worrisome body angles for a limited duration or safer body angles for longer time windows, requiring different managerial approaches. While the former can be addressed with visual management instructions, the latter suggests the need to redesign the entire workstation or even the workplace. To enable an informed decision-making process, Fig. 12 depicts the evolution of the operator's back angle during the last assembly task. According to EAWS ranges, this angle influences the detection and score of three basic movements: the standing posture falls between 0° and 20°, the bending posture ranges from 20° to 60°, and the strong bending posture is beyond 60°. As depicted in Fig. 12, the majority of time-driven back angles fall within the bending range. Specifically, the standing posture lasts 39.6 s (i.e., 23.1% of the assembly activity time), and the two bending scenarios account for 120.8 and 11.1 s, respectively. These musculoskeletal-driven values indicate significant stress on the worker's physical resilience during the final assembly task, with the last part being the most critical for the operator's back. The graph in Fig. 12 demonstrates frequent bending by the worker to insert the last drawer, suggesting that placing the furniture on the floor is not ergonomically optimal. To mitigate this, plant supervisors should consider introducing a height-adjustable support for the drawer unit, aiming to maintain the operator's back angle below 20° whenever possible. Conversely, the trunk rotation posture is distinguished by an average lumbar angle of 25.5°. The high EAWS score is due to critical angle values lasting for a prolonged period of 125.5 out of 171.7 s, accounting for 73.1% of the activity duration. These metrics suggest different managerial implications compared to the bending postures. Potential trunk rotation disorders can be prevented by ensuring that frequently accessed tools and components are within easy reach.

This first ergonomic dimension is complemented in the following two sections by monitoring the Muscular and Handling Risks.

5.2. Muscular risk

This second set of EAWS-oriented KRIs delves deeper into the ergonomic analysis by examining potentially hazardous muscular efforts during the assembly tasks. While the Global Action Forces Score of 31.1 EAWS points suggests a medium overall risk, it is crucial to adopt a top-down approach to identify specific activities that may impact operators' muscular risk. The analysis begins with the RFID-enabled Activity-Driven Action Forces Score. As illustrated in Fig. 13, approximately 68.1% of the monitored activities fall within the low-risk band. The highest score among these tasks is observed in the first activity (i.e., *Mounting Plastic Plates*), which totals 22.9 EAWS points. This task involves inserting and screwing plastic plates onto the lateral axes of the drawer (see Appendix C) and does not entail significant arm exertion. However, its extended duration of 336.8 s induces some muscular stress during the final screwing phase. Further prolonging this activity would escalate the muscular risk level. Conversely, the lowest EAWS values group the manual tasks ranging from 8 to 11, where the monitored worker assembles drawers on the workstation without significant muscular activation (% VC) in the upper limbs. However, three assembly activities account for more than 100 EAWS points, requiring in-depth evaluations. In particular, the third task (i.e., *Inserting Wooden Dowels*) has the highest score, equal to 238 EAWS points. This activity involves the manual insertion of fixing dowels into the narrow axes of the drawers. Despite its brief duration of 95.3 s, it requires considerable muscular effort from the monitored operator.

The intrinsic limitation of this first KRI is its inability to highlight the most physically stressed muscular groups. To address this, the amplitude in mV of the sEMG-based muscular contraction is shown in Fig. 14 for the right (R) and left (L) upper limbs, where the colors of the denoised signals correspond to the channel-associated EAWS risk level [24]. It can be seen that both radial flexors experience significant stress over the activity time. However, focusing solely on the acquired sEMG signal fails to highlight the muscle-specific % VC. These outputs are obtained by leveraging the second algorithm branch discussed in Section 3.2.3: the computations define sliding windows and assign each of them a % VC, as reported in Fig. 15. These non-overlapping windows facilitate a detailed assessment of muscle activation during specific intervals in the assembly tasks. The comparison between the KRIs reported in Figs. 14 and 15 reveals two distinct scenarios. First, the amplitude of the R radial flexor sEMG signal is high during the initial time window, corresponding to a 66.7% VC. Second, the sEMG signal is visually intense in the last two Channel-4 windows, which, however, correspond to 5.5% and 1.5% VC. Here it is important to underline that since % VC is a function of the maximum muscle effort, large signal amplitudes do not necessarily correlate with high muscle activation. Furthermore, the third KRI (see Fig. 15) points out valuable insights on the time domain. While the muscular activation of the R forearm (i.e., 66.7% VC) is registered for 57.3 s, the L forearm accounts for 40.5% VC over the entire task. These prolonged muscular stresses are mirrored in the Muscle-Specific Action Forces Score reported in Fig. 16.

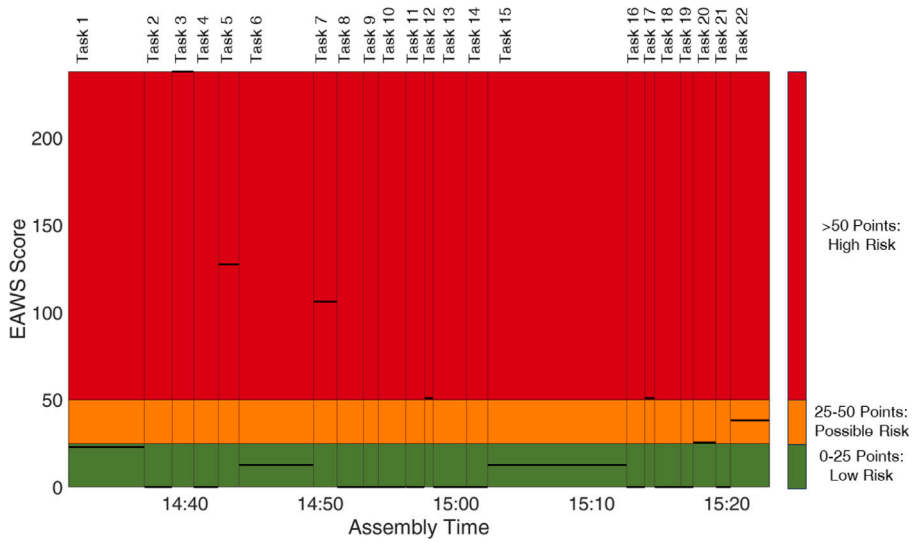

Fig. 13. Activity-Driven Action Forces Score: the sequence of tasks and their associated EAWS risk ranges are presented.

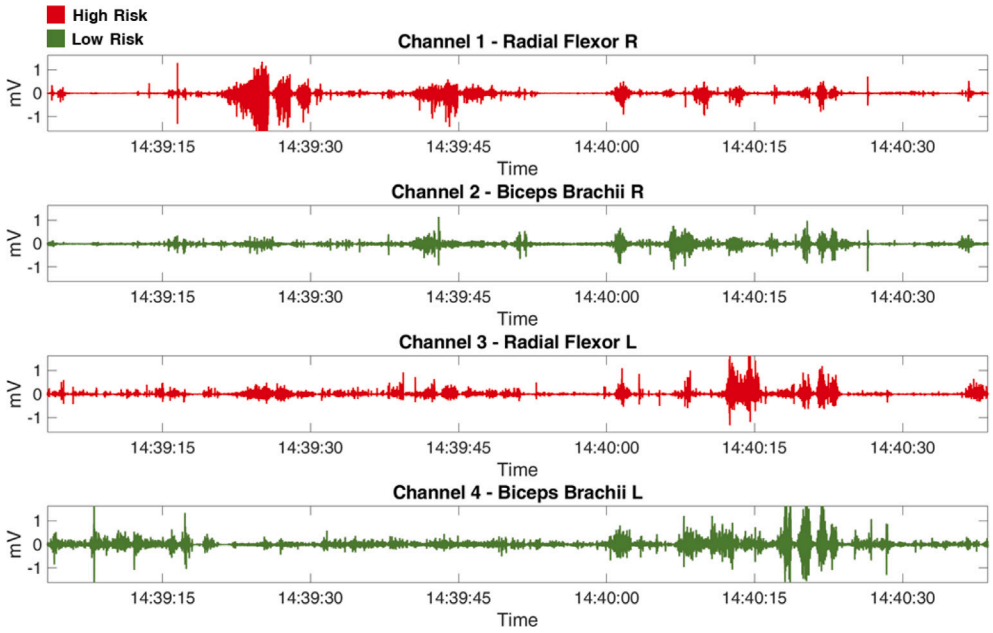

Fig. 14. EMG Raw Signal: The normalized signals recorded by the four surface electrodes positioned on the operator's upper limbs are depicted for task #3. The signals are color-coded according to the EAWS risk level associated with the channel-specific score.

While the R and L forearms accumulate 238 and 127.5 EAWS points, respectively, both biceps are green-colored since their greatest score is 17 points. It can be concluded that the risk level for the operator's forearm muscles is highly critical in this activity. The EAWS score of the right arm, likely the dominant one in this case, becomes the definitive risk measure of the task. A potential solution to lowering the analyzed score is to adopt tools that can facilitate the manual insertion of wooden dowels.

The musculoskeletal and muscular dimensions of physical resilience are finally complemented by the handling risk that quantifies the safety of workers in process-related load-lifting operations.

5.3. Handling risk

The assessment of the operator's physical resilience concludes with a discussion on Handling KRIs. Although the Global MMH Score, equal to 1.3 EAWS points, suggests a low-risk level (see Fig. 9(b)), it is essential to note that the Handling Risk is solely computed when the operator's activities involve moving, lifting, holding, pushing, or pulling loads exceeding 3 kg (refer to Section 3.2.4). In the considered assembly sequence, 4 out of 22 tasks fall into this category (i.e., tasks 7, 12, 17, and 22). Therefore, the average of the scores is not informative. Following the same top-down approach discussed in the previous risk metrics, the analysis is refined by the Activity-Driven MMH Score. Inspecting Fig. 17, it is evident that the assembly sequence considered does not report major critical MMH issues for the monitored operator, as the four relevant activities have an EAWS score lower than 25. However, proceeding with the analysis is necessary to illustrate the validity of the approach.

Fig. 17 highlights that the last task (i.e., *Mounting White Caps*) registers the highest MMH score, corresponding to 18.4 EAWS points. This task, as previously outlined in Section 5.1, entails placing two drawers inside the dresser, securing all drawers using a slotted screwdriver, and inserting the final drawer into the dresser (refer to Appendix C). As the

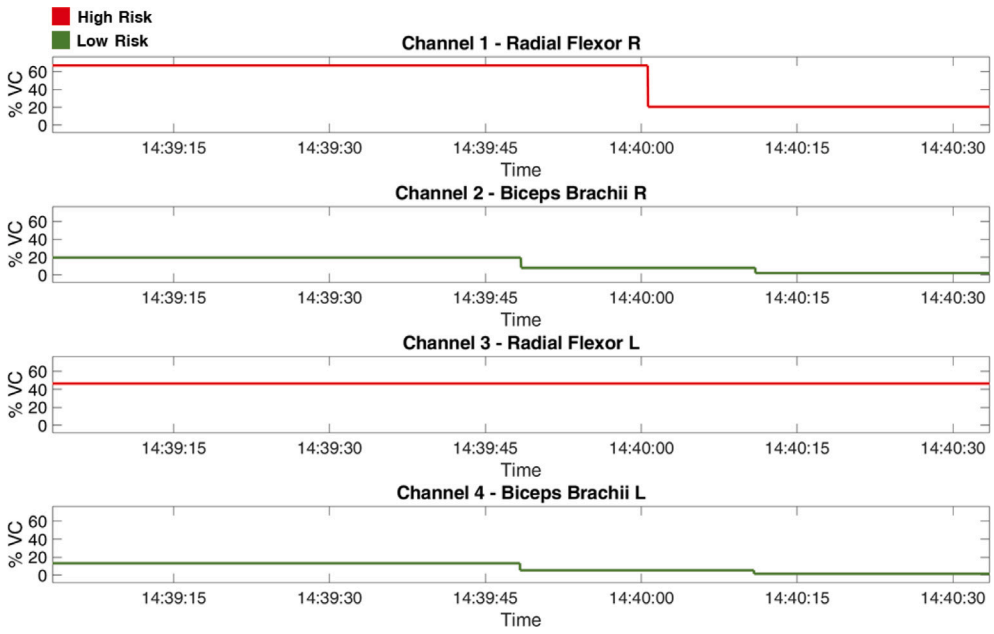

Fig. 15. Muscle-Specific and Time-Oriented % VC: The % VC computed for the four surface electrodes placed on the operator's upper limbs is depicted for task #3. The values are color-coded based on the EAWS risk level associated with the channel-specific score.

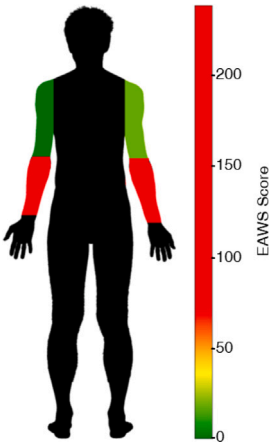

Fig. 16. Muscle-Specific Action Forces Score: The four analyzed muscle groups (i.e., radial flexors and biceps brachii) are depicted for task #3. Each group is associated with a color corresponding to the intensity of the EAWS score.

task has been already identified as critical from the musculoskeletal perspective, it is pivotal to further investigate other potential assembly-related weaknesses. For instance, Fig. 18 correlates the handled loads with the associated load points. It is worth noting that the seventh task registers the highest lifted load, which corresponds to the furniture without drawers, weighing 7.18 kg. The remaining activities (i.e., tasks 12, 17, and 22) handle the drawers and thus manage lower weights (i.e., 3 kg). Therefore, to understand why the most critical activity is the last one, it is necessary to identify the MMH time windows within this task.

The analysis narrows down to identify the muscle-dependent activation to assess the postures assumed by the operator during the MMH events. Fig. 19 presents the Muscle-Specific and Time-Oriented % VC, highlighting potentially hazardous activation in two different time windows, from 15:20:15 to 15:20:49 and from 15:22:50 to 15:23:06. In both these time intervals, the R forearm activation exceeds the MMH threshold of 16.7%, ranging from 20.7% to 17% VC. The threshold of 16.7% VC was selected as it is the minimum value necessary to attribute an intensity score to the applied forces [24]. Specifically, the analyzed KRI demonstrates two aspects. Firstly, it confirms that the radial flexor muscular group is the most stressed over the entire assembly process. To lower such activation, plant supervisors may consider purchasing lifters, or eventually cobots, to complement the physical capabilities of the workforce. Secondly, MMH events occur during both the considered time windows. In the initial time window, the operator retrieves the two previously assembled drawers from the adjacent worktable and positions them inside the dresser; in the subsequent time frame, the operator inserts the last drawer into the dresser.

The algorithm for posture detection is executed on these particular time intervals of the analyzed activity. Postures Time in MMH Windows indicates the duration of postures, obtained as a percentage of the ratio between the number of frames for which a certain movement lasts and the total frames contained in the time windows. Notably, the first three bars in Fig. 20 represent mutually exclusive postures (i.e., the percentage sum of these movements is 100), while the last four bars contain postures that can be cumulative with each other or with the first three. However, the posture considered in the final activity score is the one posing the highest risk among those assumed by the operator during the task (see Section 3.2.4). In this instance, the trunk rotation posture emerges as the most hazardous, comprising 92.3% of the total task duration, with an average critical angle of 31.3°. Although overlooked in the final score, the bending movement also has a significant impact, occupying 92% of the time with an average angle of 29.7°. These postures are the most critical in the assembly test and also affect the musculoskeletal risk perspective. Possible ergonomic enhancements include organizing tools and materials for easy access without unnatural movements, ensuring workbenches are adjusted to the correct height, and utilizing ergonomic equipment such as assisted mechanical arms to reduce the required physical effort. Additionally, raising awareness among operators about health risks associated with incorrect postures and implementing work rotation policies can help diversify tasks and reduce the repetitiveness of motion, thereby mitigating accidents.

6. Conclusions and further research

The demographic shifts in the European population, combined with an increase in the retirement age, pose significant challenges for manufacturing systems. To achieve socially inclusive working environments,

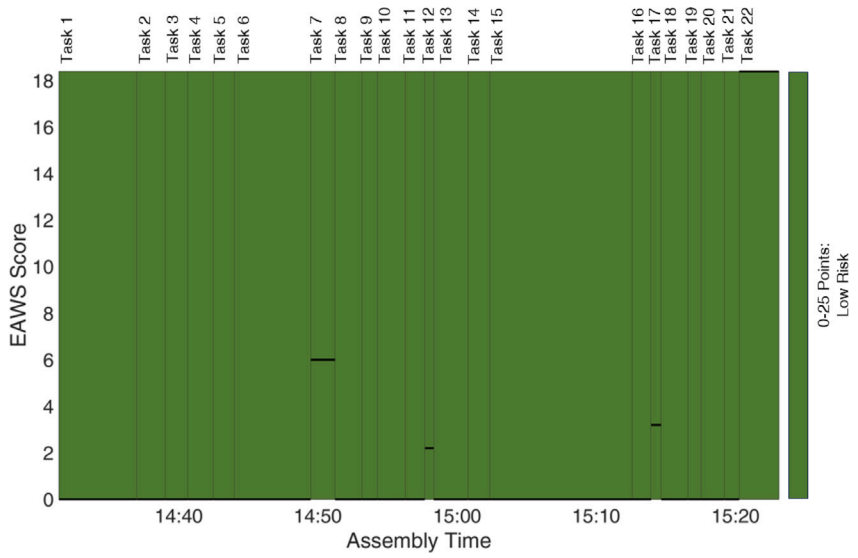

Fig. 17. Activity-Driven MMH Score: the sequence of tasks and the associated EAWS risk ranges are reported.

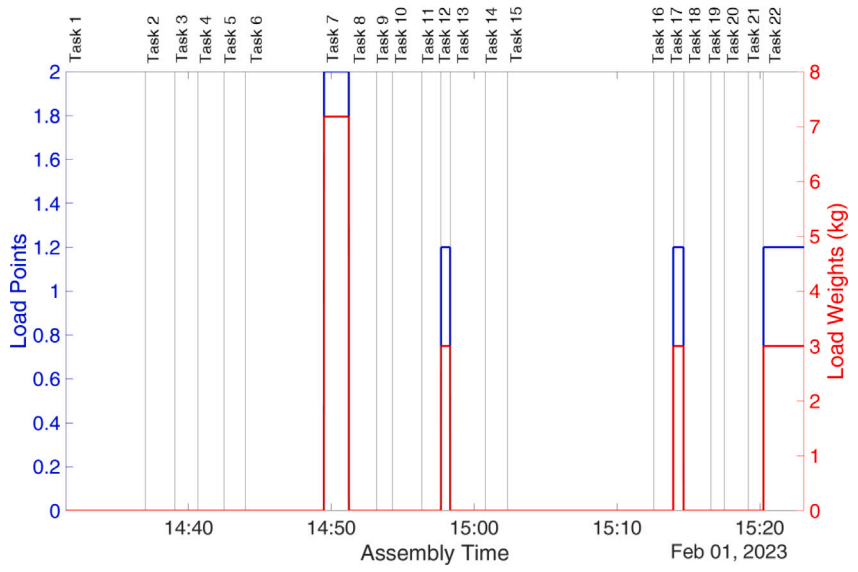

Fig. 18. Activity-Driven Load Data: the EAWS scores and weights of loads that the operator lifts during the execution of assembly tasks are provided.

Industry 5.0 triggers human-centric value creation by leveraging a diverse set of enabling technologies. Among these, Internet of Things (IoT) sensors can be utilized to monitor the physical resilience of manufacturing operators. These digital devices collect heterogeneous data streams and can be adapted to mass-customized industrial systems.

In this dynamic landscape, the objective of this research is to safeguard the physical resilience of workers by automating the computation of the European Assembly Worksheet (EAWS) in human-centric manufacturing systems. The proposed architecture digitizes the Whole Body sections of this index, namely Basic Postures, Action Forces, and Manual Material Handling. A time-dependent ergonomic decision support system is developed, integrating risk metrics that offer valuable insights for industrial process supervisors, leveraging data from three IoT devices. In particular, a Radio Frequency Identification (RFID)-based smart glove is employed to identify operator-process interactions, while motion capture (MOCAP) cameras and surface electromyography (sEMG) wearables reconstruct the operator's movements in the workspace and return upper limbs' muscular activation, respectively. By synchronizing the data from the cameras and the electromyography sensors with the smart glove data streams, both global and activity-dependent key risk indicators are evaluated. Based on these indicators, more detailed risk metrics can be derived specifically for each section of the EAWS index. The results demonstrate the capability of this innovative architecture to recognize the most risk-prone activities in the manufacturing sequence and analyze them. The digital architecture produces three types of crucial information:

1. Identification of postures with the greatest musculoskeletal risk: This aspect enables the recognition of body positions that may exert significant strain on the operator's musculoskeletal system;
2. Pinpointing muscle groups experiencing higher stress: This functionality helps identify the upper limbs' muscle groups undergoing stress during work activities, providing a detailed assessment of the physical load borne by the operator;
3. Automated recognition of manual material handling instances: The system seamlessly detects intervals when the operator is engaged in material handling tasks, providing insights into both muscular stress and body postures and reconstructing ergonomic metrics that account for these critical aspects.

Fig. 19. Muscle-Specific and Time-Oriented % VC: the graph displays the % VC computed for the four surface electrodes positioned on the operator's upper limbs for task #22. The values are color-coded based on the EAWS risk level associated with the channel-specific score, with highlighted time windows of interest.

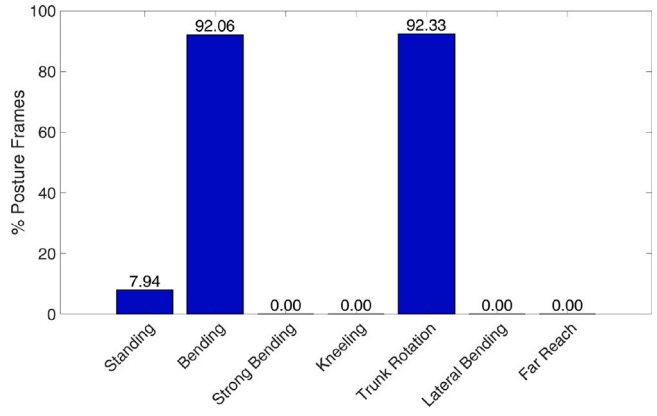

Fig. 20. Posture Time in MMH Windows: the percentage of time spent in MMH postures relative to the total duration of task #22 is reported.

Each type of information is associated with a specific risk score for the operator, allowing for a comprehensive evaluation of potential workplace hazards. Upon identifying operator-specific ergonomic weaknesses or deficiencies in the workspace setup, tailored managerial strategies can be implemented to reduce the risk level of the assembly sequence.

Although the presented digital architecture shows promising results in automating EAWS evaluations, further research opportunities can enhance and complete this development stage from various perspectives. Starting with the enabling IoT technologies, the accuracy and resolution of the MOCAP network may be compromised by occlusions, potentially leading to inaccurate estimations of body joint positions. Extensive investigations are needed to thoroughly test the accuracy of the MOCAP network. The wearability of sEMG sensors should be improved to enhance comfort for long-term use and minimize potential interference during manual tasks. For example, a smart EMG-based t-shirt could be a promising solution [61]. Additionally, the acquisition IoT layer should capture the motion patterns of hands and wrists to digitize the fourth EAWS section (i.e., Upper Limb Load in Repetitive Tasks). Despite the amount of digitized EAWS sections, the ergonomic screening tool does not comprehensively evaluate workers' well-being. Additional methods should be explored to integrate mental workload analysis. Lastly, a human-centric digital twin should be developed to complement the current architecture's operational mode (i.e., offline). By benefiting from real-time feedback loops, users can appreciate several advantages. Supervisors can more promptly identify and mitigate ergonomic risks, while early warnings can suggest optimal behaviors for workers to reduce such risks in the short term.

CRediT authorship contribution statement

Federica Tomelleri: Writing – review & editing, Writing – original draft, Visualization, Validation, Software, Methodology, Investigation, Formal analysis, Data curation, Conceptualization. **Andrea Sbaragli:** Writing – review & editing, Writing – original draft, Visualization, Validation, Software, Methodology, Investigation, Formal analysis, Data curation, Conceptualization. **Francesco Picariello:** Writing – review & editing, Writing – original draft, Supervision, Software, Resources. **Francesco Pilati:** Writing – review & editing, Supervision, Resources, Project administration, Conceptualization.

Declaration of competing interest

The authors declare that they have no known competing financial interests or personal relationships that could have appeared to influence the work reported in this paper.

Appendix A

This appendix provides the nomenclature, divided into indices and parameters, to facilitate the reading process. Please note that both indices and parameters are alphabetically ordered.

Indices $a = 1, \dots, A$: Activity of the assembly sequence
$b = 1, \dots, B$: Kinect body joints
$c = 1, 2$: Kinect camera
$f = 1, \dots, F$: RFID-based scanning frame of activity passive tags
$f' = 1, \dots, F'$: RFID-based scanning frame of tool passive tags
$g, g' = 1, \dots, G$: Body joint groups
$i = 1, \dots, I$: Acquisition frame of the BITalino board
$k = 1, \dots, K$: Kinect recording frame
$m = 1, \dots, 4$: sEMG acquisition channels or recording muscles
$n = 1, \dots, N$: sEMG acquisition in the initialization stage

$p = 1, \dots, P$: EAWS basic postures
$r = 1, \dots, R$: Temporal occurrence of EAWS posture
$s = 1, \dots, 4$: EAWS manual material handling postures
$t = 1, \dots, T$: Tool usage
$v, v' = 1, \dots, V$: Relevant manual material handling event
$w = 1, \dots, W$: Overlapping sliding window
Parameters α: Hyper-parameter to discard tool usage
τ: Hyper-parameter to merge consecutive tool usage
δ: Sampling frequency of the adopted RFID-based smart glove
$\Theta^a_{g-g',k}$: Angle between the muscular body joint groups g and g' during the kth Kinect frame for the ath assembly activity
$ADAFS^a$: Activity-driven Action Force Score for the ath assembly activity
$ADBPS^a_m$: Activity-driven Basic Posture Score for the mth muscle during the ath assembly activity
$ADBPS^a$: Activity-driven Basic Posture Score during the ath assembly activity
$AMMC_{m,w}$: Absolute magnitude of muscular contractions for the mth channel during the wth sliding window
$ADMMHS^a$: Activity-driven Manual Material Handling Score during the ath assembly activity
AS_f: Activity-related passive RFID string scanned during the fth frame
AT_f: Timestamp related to AS_f
$CL^c_{b,k}$: Confidence level related to $Pos^c_{b,k}$
D^a_p: Duration of holding the pth EAWS posture during the ath assembly activity
$D^a_{p,r}$: Duration of holding the pth EAWS posture for the rth occurrence during the ath assembly activity
D^n_m: Duration to achieve the MVC for the mth channel and nth acquisition
D_m: Duration to achieve the MVC for the mth channel
$DMMC_{m,w}$: Duration related to the absolute magnitude of muscular contractions for the mth channel during the wth sliding window
D^a_v: Duration of the vth manual material handling event during the ath assembly activity
$DFScore^a_{m,w}$: EAWS Duration Force Score for the mth channel during the wth sliding window and ath assembly activity
$FScore^a_{m,w}$: EAWS Action Force Score for the mth channel during the wth sliding window and ath assembly activity
F_v: Repetition rate of the vth material handling event over the entire working cycle
$GAFS$: Global Action Force Score
$GBPS$: Global Basic Posture Score
$GMMHS$: Global Manual Material Handling Score
$MA_{m,w}$: Muscular activation for the mth channel during the wth sliding window
$MA^a_{m,w}$: Muscular activation for the mth channel during the wth sliding window and ath assembly activity
MVC^n_m: Maximal voluntary contraction for the mth channel and nth acquisition
MVC_m: Maximal voluntary contraction for the mth channel
$MMHPS^a_{s,v}$: EAWS Score related to the sth posture during the vth manual material handling event and ath assembly activity
$MMHPS^a_v$: EAWS Posture Score during the vth manual material handling event and ath assembly activity
$MMHFS_v$: EAWS Score related to F_v
$noise^n_m$: sEMG acquisition noise in resting scenarios for the mth channel and nth acquisition
$noise_m$: sEMG acquisition noise in resting scenarios for the mth channel
$over_m$: Duration of overlap of the sliding windows for the mth channel
$Pos_{b,k}$: Reconstructed 3D position for the bth body joint during the kth Kinect frame

Table B.3
Posture-dependent body joints.

Posture	Body joint group	Number
Walking	Pelvis	1
Standing	Back	1, 2, 3, 4
	Leg (R)	1, 23, 24, 25
	Leg (L)	1, 19, 20, 21
Low Bending (20 – 60°)	Back	1, 2, 3, 4
	Leg (R)	1, 23, 24, 25
	Leg (L)	1, 19, 20, 21
High Bending (> 60°)	Back	1, 2, 3, 4
	Leg (R)	1, 23, 24, 25
	Leg (L)	1, 19, 20, 21
Elbows Above Shoulders	Back	1, 2, 3, 4
	Arm (R)	12, 13, 14, 15
	Arm (L)	5, 6, 7, 8
Hands Above Head	Back	1, 2, 3, 4
	Arm (R)	12, 13, 14, 15
	Arm (L)	5, 6, 7, 8
Upright (Kneeling)	Back	1, 2, 3, 4
	Knee (R)	23, 24
	Knee (L)	19, 20
	Ankle (R)	24, 25
	Ankle (L)	20, 21
Bent Forward (Kneeling)	Back	1, 2, 3, 4
	Knee (R)	23, 24
	Knee (L)	19, 20
	Ankle (R)	24, 25
	Ankle (L)	20, 21
Elbows Above Shoulders (Kneeling)	Knee (R)	23, 24
	Knee (L)	19, 20
	Ankle (R)	24, 25
	Ankle (L)	20, 21
	Arm (R)	12, 13, 14, 15
	Arm (L)	5, 6, 7, 8
Trunk Rotation (Asymmetric)	Spine Naval, Hips	2, 19, 23
	Spine Chest, Shoulders	3, 6, 13
Lateral Bending (Asymmetric)	Back	1, 2, 3, 4
	Hip (R)	1, 23
Far Reach (Asymmetric)	Arm (R)	12, 13, 14, 15
	Arm (L)	5, 6, 7, 8

$Pos^c_{b,k}$: 3D body position of the bth body joint during the kth Kinect frame for the cth camera
S_a: Passive assembly tag of the ath assembly activity
S_t: Passive tool tag of the tth assembly activity
$Scan_a$: Scanning list of AT_f belonging to the same ath assembly activity
$Scan_t$: Scanning list of $TT_{f'}$ belonging to the same tth tool usage
T_a: Starting timestamp of the ath assembly activity
$TS_{f'}$: Tool-related passive RFID string scanned during the f'th frame
$Tstart^a_p$: Starting timestamp of D^a_p
$Tend^a_p$: Ending timestamp of D^a_p
$TT_{f'}$: Timestamp related to $TS_{f'}$
$TTstart_t$: Starting timestamp related to the tth tool usage
$TTend_t$: Ending timestamp related to the tth tool usage
$Tstart^a_v$: Starting timestamp related to the vth manual material handling event
$Tend^a_v$: Ending timestamp related to the vth manual material handling event
thr_m: Threshold value for the mth channel
$V^a_{g,k}$: Vectorial structure of the gth body joint group during the kth Kinect frame for the ath assembly activity
$Wdur_m$: Duration of the overlapping sliding windows for the mth channel
WS^a: EAWS Weight Score related to the ath assembly activity
$x_{i,m}$: sEMG during the ith acquisition frame for the mth channel

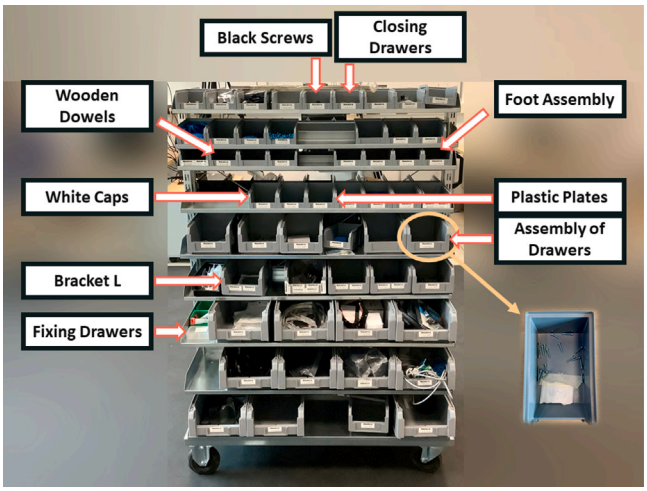

Fig. C.21. Layout of the supermarket showing the locations of components required for the different assembly tasks.

x_a: Binary variable associated with MMH events
$\%\ VC_m$: Percentage of voluntary contraction for the mth channel
$\%VC_{m,w}$: Percentage of voluntary contraction for the mth channel during the wth sliding window
$\%VC^a_{m,w}$: Percentage of voluntary contraction for the mth channel during the wth sliding window and ath assembly activity

Appendix B

This Appendix lists the posture-dependent body joints, as detailed in Table B.3.

Appendix C

This appendix details the sequence of activities performed by the operator during the assembly of the dresser. At the beginning of each task, the operator retrieves the necessary components from the supermarket, as illustrated in Fig. C.21. The tools are already conveniently positioned on the table of the workstation.

Task ID - Assembly Process Activities

- **Task 1 - Mounting Plastic Plates**: Collect screws and plastic plates, and place them on the worktable. Retrieve two wooden panels (i.e., the sides of the dresser) from under the table and place them on top. Position the sliding plates on the wooden panels and secure them with screws using a Phillips screwdriver, as indicated in Fig. C.22(a). Move the panels aside to make space on the table.
- **Task 2 - Mounting Bracket L**: Collect L-brackets and fastening screws, and place them on the worktable. Retrieve a third wooden panel (i.e., the back of the dresser) from under the table and place it on top. Position the L-brackets on the wooden panel and secure them with screws using a Phillips screwdriver, as indicated in Fig. C.22(b).
- **Task 3 - Inserting Wooden Dowels**: Collect wooden dowels and stand in front of the worktable. Manually insert the dowels into the sides of the back panel of the dresser as indicated in Fig. C.22(c).
- **Task 4 - Tightening Black Screws**: Collect black screws and place them on the worktable. Retrieve two wooden panels (i.e., a side and the back of the dresser) and align them. Secure the two parts with black screws using a hexagonal Allen key as depicted in Fig. C.22(d). Move the semi-assembled piece aside to make space on the table.
- **Task 5 - Inserting Wooden Dowels**: Collect additional wooden dowels and place them on the worktable. Retrieve two thin wooden panels (i.e., the supports of the dresser) from under the table and place them on top. Manually insert the wooden dowels into the indicated spots as in Fig. C.22(e) and move the supports aside to make space on the table.
- **Task 6 - Tightening Black Screws**: Collect more black screws and place them on the worktable. Bring the semi-assembled piece and the two support panels closer, fitting the pieces one at a time. Secure the various parts with black screws using a hexagonal Allen key. Align the remaining wooden panel (i.e., the other side of the dresser) with the semi-assembled piece and secure it with black screws using a hexagonal Allen key (see Fig. C.22(f)).
- **Task 7 - Foot Assembly**: Collect the specific nails and place them on the worktable. Lift, turn, and move the semi-assembled dresser to the floor to secure the nails with a hammer (see Fig. C.22(g)). Turn and reposition the dresser upright on the floor.
- **Task 8 - Assembly of Drawer (1)**: Collect appropriate screws and place them on the worktable. Retrieve a thin wooden panel (i.e., the outer face of the drawer) from under the table and place it on top. Secure the screws with a Phillips screwdriver in the spots indicated in Fig. C.22(h) to allow the insertion of the drawer's side panels.
- **Task 9 - Inserting Wooden Dowels (1)**: Collect additional wooden dowels and place them on the worktable. Retrieve two thin wooden panels (i.e., the sides of the drawer) from under the table and place them on top. Manually insert the dowels into the appropriate spots and slide the drawer's side panels onto the previously screwed front panel as in Fig. C.22(i).
- **Task 10 - Fixing Drawer (1)**: Collect appropriate screws and insert them into the drawer's side panels using a slotted screwdriver, securing them to the previously prepared front panel (see Fig. C.22(j)). Retrieve the drawer base and back panel, slide the base into the slots inside, and fit the back panel into the free part of the base.
- **Task 11 - Closing Drawer (1)**: Collect specific nails and secure the drawer back with a hammer, fitting the side panels with the closing panel as indicated in Fig. C.22(k).
- **Task 12 - Mounting White Caps (1)**: Collect white screws and manually insert them into the drawer's side panels without fully securing them. Move the drawer to the adjacent worktable to make space on the main table.
- **Task 13 - Assembly of Drawer (2)**: Repeat the same steps as Task 8 for the second drawer.
- **Task 14 - Inserting Wooden Dowels (2)**: Repeat the same steps as Task 9 for the second drawer.
- **Task 15 - Fixing Drawer (2)**: Repeat the same steps as Task 10 for the second drawer.
- **Task 16 - Closing Drawer (2)**: Repeat the same steps as Task 11 for the second drawer.
- **Task 17 - Mounting White Caps (2)**: Repeat the same steps as Task 12 for the second drawer.
- **Task 18 - Assembly of Drawer (3)**: Repeat the same steps as Task 8 for the third drawer.
- **Task 19 - Inserting Wooden Dowels (3)**: Repeat the same steps as Task 9 for the third drawer.
- **Task 20 - Fixing Drawer (3)**: Repeat the same steps as Task 10 for the third drawer.
- **Task 21 - Closing Drawer (3)**: Repeat the same steps as Task 11 for the third drawer.
- **Task 22 - Mounting White Caps (3)**: Collect white screws and manually insert them into the third drawer's side panels without fully securing them. Retrieve the two previously assembled drawers from the adjacent worktable and place them inside the dresser (see Fig. C.22(l)). Secure the already inserted drawers in the dresser using a slotted screwdriver, then secure the white

(a) Task 1 (b) Task 2 (c) Task 3 (d) Task 4

(e) Task 5 (f) Task 6 (g) Task 7 (h) Task 8

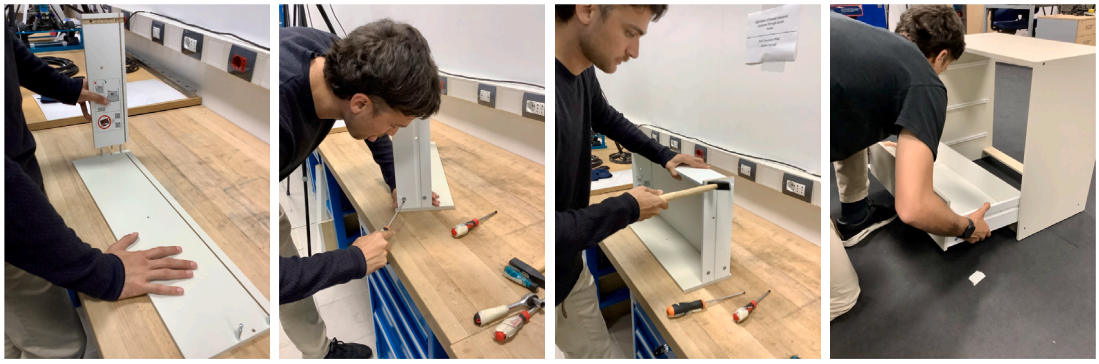

(i) Task 9 (j) Task 10 (k) Task 11 (l) Task 22

(m) Tools

Fig. C.22. Visual representation of assembly tasks, showcasing the operator's interactions with components and tools at different stages.

screws on the last drawer. Insert the last drawer into the dresser, completing the assembly process. *Note*: Securing all the drawers at the end optimizes tool usage. Securing two drawers inside and one on the table is for the operator's convenience.

The tools used by the operator during the assembly process are illustrated in Fig. C.22(m).

References

[1] European Commission, Directorate-General for Research and Innovation, Müller J. Enabling technologies for industry 5.0 : results of a workshop with Europe's technology leaders. Publications Office; 2020.

[2] Eurostat. Ageing Europe—statistics on population developments. 2023, https://ec.europa.eu/eurostat/statistics-explained/index.php?title=Ageing_Europe_-_statistics_on_population_developments [Accessed 3 November 2023].

[3] Chatzoudes D, Chatzoglou P. Factors affecting employee retention: Proposing an original conceptual framework. Int J Econ Bus Adm 2022;10(1):49–76.

[4] Cedefop. Job turnover. 2021, https://www.cedefop.europa.eu/en/tools/skills-intelligence/job-turnover?year=2021&country=EU#1 [Accessed 10 November 2023].

[5] Suzic N, Forza C. Development of mass customization implementation guidelines for small and medium enterprises (SMEs). Prod Plan Control 2023;34(6):543–71.

[6] Pilati F, Sbaragli A, Ruppert T, Abonyi J. Goal-oriented clustering algorithm to monitor the efficiency of logistic processes through real-time locating systems. Int J Comput Integr Manuf 2024;1–17.

[7] Shi Z, Xie Y, Xue W, Chen Y, Fu L, Xu X. Smart factory in industry 4.0. Syst Res Behav Sci 2020;37(4):607–17.

[8] Barbosa WS, Gioia MM, Natividade VG, Wanderley RF, Chaves MR, Gouvea FC, Gonçalves FM. Industry 4.0: examples of the use of the robotic arm for digital manufacturing processes. Int J Interact Des Manufact 2020;14:1569–75.

[9] Albanese A, Brunelli D. Industrial visual inspection with TinyML for high-performance quality control. IEEE Instrument Measur Mag 2023.

[10] Slovák J, Vašek P, Šimovec M, Melicher M, Šišmišová D. RTLS tracking of material flow in order to reveal weak spots in production process. In: 2019 22nd international conference on process control. IEEE; 2019, p. 234–8.

[11] Santoro L, Nardello M, Brunelli D, Fontanelli D. UWB-based indoor positioning system with infinite scalability. IEEE Trans Instrum Meas 2023.

[12] Huang S, Wang B, Li X, Zheng P, Mourtzis D, Wang L. Industry 5.0 and society 5.0—Comparison, complementation and co-evolution. J Manufact Syst 2022;64:424–8.

[13] Pilati F, Sbaragli A. Learning human-process interaction in manual manufacturing job shops through indoor positioning systems. Comput Ind 2023;151:103984.

[14] Pilati F, Sbaragli A, Tomelleri F, Picariello E, Picariello F, Tudosa I, Nardello M. Operator 5.0: enhancing the physical resilience of workers in assembly lines. In: 2023 IEEE international workshop on metrology for industry 4.0 & ioT. IEEE; 2023. p. 177–82.

[15] Ivanov D. The industry 5.0 framework: Viability-based integration of the resilience, sustainability, and human-centricity perspectives. Int J Prod Res 2023;61(5):1683–95.

[16] Xu X, Lu Y, Vogel-Heuser B, Wang L. Industry 4.0 and industry 5.0—Inception, conception and perception. J Manuf Syst 2021;61:530–5.

[17] Golovianko M, Terziyan V, Branytskyi V, Malyk D. Industry 4.0 vs. industry 5.0: Co-existence, transition, or a hybrid. Procedia Comput Sci 2023;217:102–13.

[18] Romero D, Stahre J. Towards the resilient operator 5.0: The future of work in smart resilient manufacturing systems. Proc CIRP 2021;104:1089–94.

[19] De Vito L, Picariello E, Picariello F, Rapuano S, Tudosa I, Sbaragli A, Pilati F. IoT-based system for monitoring the well-being of industrial operators through wearable devices. In: 2024 IEEE international symposium on medical measurements and applications. IEEE; 2024, p. 1–6.

[20] Gladysz B, Tran T-a, Romero D, van Erp T, Abonyi J, Ruppert T. Current development on the operator 4.0 and transition towards the operator 5.0: A systematic literature review in light of industry 5.0. J Manuf Syst 2023;70:160–85.

[21] Wang B, Zheng P, Yin Y, Shih A, Wang L. Toward human-centric smart manufacturing: A human-cyber-physical systems (HCPS) perspective. J Manuf Syst 2022;63:471–90.

[22] de Vito L, Picariello E, Picariello F, Tudosa I, Loprevite L, Avicolli D, Laudato G, Oliveto R. An undershirt for monitoring of multi-lead ECG and respiration wave signals. In: 2021 IEEE international workshop on metrology for industry 4.0 & ioT. 2021. p. 550–5. 10.1109/MetroInd4.0IoT51437.2021.9488547.

[23] De Vito L, Picariello E, Picariello F, Tudosa I, Sbaragli A, Papini GPR, Pilati F. Measurement system for operator 5.0: a learning fatigue recognition based on sEMG signals. In: 2023 IEEE international symposium on medical measurements and applications. 2023, p. 1–6. http://dx.doi.org/10.1109/MeMeA57477.2023.10171933.

[24] Schaub K, Caragnano G, Britzke B, Bruder R. The European assembly worksheet. Theor Issues Ergon Sci 2013;14(6):616–39.

[25] Mourtzis D, Angelopoulos J, Panopoulos N. Operator 5.0: A survey on enabling technologies and a framework for digital manufacturing based on extended reality. J Mach Eng 2022;22.

[26] Romero D, Stahre J. Towards the resilient operator 5.0: The future of work in smart resilient manufacturing systems. Proc CIRP 2021;104:1089–94.

[27] Ayvaz S, Alpay K. Predictive maintenance system for production lines in manufacturing: A machine learning approach using IoT data in real-time. Expert Syst Appl 2021;173:114598.

[28] Brunner O, Mertens A, Nitsch V, Brandl C. Accuracy of a markerless motion capture system for postural ergonomic risk assessment in occupational practice. Int J Occup Saf Ergon 2022;28(3):1865–73.

[29] Rahman MM, Sarkar AK, Hossain MA, Hossain MS, Islam MR, Hossain MB, Quinn JM, Moni MA. Recognition of human emotions using EEG signals: A review. Comput Biol Med 2021;136:104696.

[30] Jiao J, Zhou F, Gebraeel NZ, Duffy V. Towards augmenting cyber-physical-human collaborative cognition for human-automation interaction in complex manufacturing and operational environments. Int J Prod Res 2020;58(16):5089–111.

[31] Cimen T, Baykasoğlu A, Akyol S. Assembly line rebalancing and worker assignment considering ergonomic risks in an automotive parts manufacturing plant. Int J Indus Eng Comput 2022;13(3):363–84.

[32] Occhipinti E, Colombini D. The occupational repetitive action (OCRA) methods: OCRA index and OCRA checklist. Handb Hum Factors Ergon Methods 2005;1–14.

[33] Waters TR, Putz-Anderson V, Garg A, Fine LJ. Revised NIOSH equation for the design and evaluation of manual lifting tasks. Ergonomics 1993;36(7):749–76.

[34] Spitzhirn M, Kuhlang P, Bullinger AC. Digitalization of the ergonomic assessment worksheet–user requirements for EAWS digital evaluation functions. In: Proceedings of the 20th congress of the international ergonomics association (IEA 2018) volume VII: ergonomics in design, design for all, activity theories for work analysis and design, affective design 20. Springer; 2019, p. 272–82.

[35] Matt DT, Rauch E. Designing assembly lines for mass customization production systems. Mass Cust Manuf Theor Concepts Pract Approaches 2017. 9781315398983–3.

[36] Caputo F, Greco A, D 'Amato E, Notaro I, Spada S. Imu-based motion capture wearable system for ergonomic assessment in industrial environment. In: Advances in human factors in wearable technologies and game design: proceedings of the AHFE 2018 international conferences on human factors and wearable technologies, and human factors in game design and virtual environments, held on July 21–25, 2018, in loews sapphire falls resort at universal studios, orlando, florida, USA 9. Springer; 2019, p. 215–25.

[37] Kim W, Huang C, Yun D, Saakes D, Xiong S. Comparison of joint angle measurements from three types of motion capture systems for ergonomic postural assessment. In: Advances in physical, social & occupational ergonomics: proceedings of the AHFE 2020 virtual conferences on physical ergonomics and human factors, social & occupational ergonomics and cross-cultural decision making, July 16–20, 2020, USA. Springer; 2020, p. 3–11.

[38] Tran T-a, Ruppert T, Eigner G, Abonyi J. Assessing human worker performance by pattern mining of Kinect sensor skeleton data. J Manuf Syst 2023;70:538–56.

[39] Desmarais Y, Mottet D, Slangen P, Montesinos P. A review of 3D human pose estimation algorithms for markerless motion capture. Comput Vis Image Underst 2021;212:103275.

[40] Kanko RM, Laende EK, Davis EM, Selbie WS, Deluzio KJ. Concurrent assessment of gait kinematics using marker-based and markerless motion capture. J Biomech 2021;127:110665.

[41] Bao S, Spielholz P, Howard N, Silverstein B. Force measurement in field ergonomics research and application. Int J Ind Ergon 2009;39(2):333–40.

[42] Paulsen R, Gallu T, Gilkey D, Reiser II R, Murgia L, Rosecrance J. The inter-rater reliability of Strain ?index and OCRA checklist task assessments in cheese processing. Appl Ergon 2015;51:199–204.

[43] David GC. Ergonomic methods for assessing exposure to risk factors for work-related musculoskeletal disorders. Occup Med 2005;55(3):190–9.

[44] Konrad P. The abc of EMG. A Pract Introd Kinesiol Electromyogr 2005;1.

[45] Chaiklieng S, Poochada W. Assessment of muscle fatigue and potential health risk of low back pain among call center workers. In: Advances in physical, social & occupational ergonomics: proceedings of the AHFE 2021 virtual conferences on physical ergonomics and human factors, social & occupational ergonomics, and cross-cultural decision making, July 25-29, 2021, USA. Springer; 2021, p. 54–61.

[46] Avdan G, Onal S, Smith BK. Normalization of EMG signals: Optimal MVC positions for the lower limb muscle groups in healthy subjects. J Med Biol Eng 2023;43(2):195–202.

[47] Akinnola OO, Vardakastani V, Kedgley AE. Identifying tasks to elicit maximum voluntary contraction in the muscles of the forearm. J Electromyogr Kinesiol 2020;55:102463.

[48] Dahlqvist C, Nordander C, Granqvist L, Forsman M, Hansson G-Ak. Comparing two methods to record maximal voluntary contractions and different electrode positions in recordings of forearm extensor muscle activity: Refining risk assessments for work-related wrist disorders. Work 2018;59(2):231–42.

[49] Rajendran M, Sajeev A, Shanmugavel R, Rajpradeesh T. Ergonomic evaluation of workers during manual material handling. Mater Today Proc 2021;46:7770–6.

[50] Pratiwi I, Hartanto H. Manual material handling analysis of work posture in biomemechanics aspect using key indicator method (KIM) and ergonomic assessment worksheet (EAWS) in barecore workers. In: AIP conference proceedings, vol. 2727. AIP Publishing; 2023.
[51] Lunin A, Glock CH. Systematic review of Kinect-based solutions for physical risk assessment in manual materials handling in industrial and laboratory environments. Comput Ind Eng 2021;162:107660.
[52] Musa A, Dabo A-AA. A review of RFID in supply chain management: 2000–2015. Global J Flexible Syst Manag 2016;17(2):189–228.
[53] Arkan I, Van Landeghem H. Evaluating the performance of a discrete manufacturing process using RFID: A case study. Robot Comput-Integr Manuf 2013;29(6):502–12.
[54] Singh RK, Michel A, Nepa P, Salvatore A. Glove integrated dual-band Yagi reader antenna for UHF RFID and bluetooth application. In: 2020 international workshop on antenna technology. IEEE; 2020. p. 1–3.
[55] Pycom. PyScan. 2023, https://docs.pycom.io/datasheets/expansionboards/pyscan/ [Accessed 20 November 2023].
[56] Guerreiro J, Lourenço A, Silva H, Fred A. Performance comparison of low-cost hardware platforms targeting physiological computing applications. Proc Technol 2014;17:399–406. http://dx.doi.org/10.1016/j.protcy.2014.10.204, Conference on electronics, telecommunications and computers–CETC 2013.
[57] Azure kinect DK fact sheet. 2023, https://news.microsoft.com/wp-content/uploads/prod/2019/06/Factsheet-Azure-Kinect-DK.pdf [Accessed 5 December 2023].
[58] Kroemer K, Marras WS. Towards an objective assessment of the "maximal voluntary contraction" component in routine muscle strength measurements. Eur J Appl Physiol Occup Physiol 1980;45:1–9.
[59] Andersen KS, Christensen BH, Samani A, Madeleine P. Between-day reliability of a hand-held dynamometer and surface electromyography recordings during isometric submaximal contractions in different shoulder positions. J Electromyography Kinesiol 2014;24(5):579–87.
[60] Kareem G. Lower limb sEMG denoising using daubechies wavelets. Int J Intell Comput Inform Sci 2023;23(2):145–56.
[61] Picariello F, Tudosa I, Balestrieri E, Daponte P, Rapuano S, De Vito L. Atticus: A novel wearable system for physiological parameters monitoring. In: AISEM annual conference on sensors and microsystems. Springer; 2020, p. 157–65.